UNIVERSITY OF CALIFORNIA SAN DIEGO

Silicon and silicon oxide: Investigation of full cells, binder additive, and pre-lithiation for Li-ion batteries

A Thesis submitted in partial satisfaction of the requirements for the degree Master of Science

in

Materials Science and Engineering

by

Macwin Savio Dsouza

Committee in charge:

Professor Ying Shirley Meng, Chair
Professor Ping Liu, Co-Chair
Professor Zheng Chen

2019

The Thesis of Macwin Savio Dsouza is approved, and it is acceptable in quality and form for publication on microfilm and electronically:

_____

_____
Co-Chair

_____
Chair

University of California San Diego

2019

DEDICATION

This thesis is dedicated to my parents,

Cynthia and *Michael,*

and my brother, *Menald*.

EPIGRAPH

There are things you can’t see unless you change your standing.

Eiichiro Oda

TABLE OF CONTENTS

LIST OF ABBREVIATIONS

LIB	Lithium-ion batteries
CO_2	Carbon Dioxide
Si	Silicon
SEI	Solid Electrolyte Interface
SiO_x	Silicon Oxide
SLMP	Stabilized Lithium Metal Powder
CMC-Na	Sodium Carboxymethyl Cellulose
-COOH	Carboxyl group
PAA	Poly Acrylic Acid
Cu	Copper
NMC111	Lithium Nickel (Ni) Manganese (Mn) Cobalt (Co) Oxide (Ni:Mn:Co = 1:1:1)
PVDF	Polyvinylidene Fluoride
NMP	N-methyl-2-pyrrolidone
$LiPF_6$	Lithium Hexafluorophosphate
EC/DEC/FEC	Ethylene Carbonate/Diethyl Carbonate/Fluoroethylene Carbonate
Li	Lithium
OCV	Open Circuit Voltage
DMC	Dimethyl Carbonate
XRD	X-Ray Diffraction
SEM	Scanning Electron Microscope
KB	Ketjenblack Carbon

CE	Coulombic Efficiency
RE	Reference Electrode
N/P	Ratio of Anode Capacity to Cathode Capacity
O_2	Oxygen gas
SOC	State of Charge
R_B	Bragg Factor
R_{wp}	Weighted Profile R-factor
MO_2	Transition Metal and Oxygen Layer (M is $Ni_{1/3}Mn_{1/3}Co_{1/3}$)
$LiFePO_4$	Lithium Iron (Fe) Phosphate
$LiNi_{0.5}Mn_{1.5}O_4$	Lithium Nickel (Ni) Manganese (Mn) Oxide
hFTN	Human Ferritin Heavy Chain
LiOH	Lithium Hydroxide
Li-PAA	Lithium Polyacrylate Binder
Li_2CO_3	Lithium Carbonate
EDS	Energy Dispersive X-Ray Spectroscopy
C	Carbon
O	Oxygen
SiO	Silicon Monoxide
Li_4SiO_4	Lithium Orthosilicate
Li_2O	Lithium Oxide
Al	Aluminum

LIST OF SYMBOLS

μ	Micrometer
α	Alpha
θ	Theta

LIST OF FIGURES

LIST OF TABLES

ACKNOWLEDGMENTS

I am especially grateful to my family. Without their love and support, this journey would not have been possible.

I would like to acknowledge Prof. Ying Shirley Meng for her guidance and support as the chair of my committee. The research journey at her lab was by far the best experience of my life so far. I have only her to thank for providing such a wonderful opportunity.

I would also like to acknowledge Dr. Abhik Banerjee and Dr. Pritesh Parikh without whom my research would have no doubt taken five times as long. It is their support that helped me in an immeasurable way.

I would like to thank Kenneth Han from Tezcan lab for being a great collaborator for the Ferritin project.

I would like to thank Øystein Fjeldberg and Jonathan Scharf for being great friends and partaking in all the discussions that helped me be a better person.

I would like to specially thank Dr. Dijo Damien, Hyeseung Haelie Chung, Erik Wu, and Shuang Bai for their help throughout my time whenever I had queries.

I would also like to thank all the Laboratory for Energy Storage and Conversion (LESC) members for their unique technical skills that I could learn from and making LESC a great place to work.

I would also like to acknowledge all my committee members, Prof. Ping Liu, and Prof. Zheng Chen for their support and suggestions that have strengthened this thesis.

I would like to thank UC San Diego for providing an excellent facility to carry out this work. All the SEM/EDS in this work was performed at the San Diego Nanotechnology Infrastructure (SDNI), a member of the National Nanotechnology Coordinated Infrastructure, which is supported by the National Science Foundation (Grant ECCS-1542148). XRD measurements were performed at UCSD Crystallography Facility and Center for Memory and Recording Research (CMRR).

Chapter 2 is coauthored with Dr. Pritesh Parikh, Dr. Abhik Banerjee, Osman Trieu, Yongbai Josh Gong, and Prof. Ying Shirley Meng. The thesis author is the primary author of this chapter.

Chapter 3 is coauthored with Kenneth Han, Dr. Dijo Damien, Dr. Pritesh Parikh, Dr. Abhik Banerjee, Osman Trieu, and Prof. Ying Shirley Meng. The thesis author is the primary author of this chapter.

Chapter 4 is coauthored with Yongbai Josh Gong, Dr. Pritesh Parikh, Dr. Abhik Banerjee, Osman Trieu, and Prof. Ying Shirley Meng. The thesis author is the primary author of this chapter.

VITA

2012-2016 Bachelor of Engineering, R. V. College of Engineering, India

2016-2017 Process Engineer, Reliance Industries Limited, India

2017-2019 Research Assistant, University of California San Diego

2019-2019 Teaching Assistant, University of California San Diego

2019 Master of Science, University of California San Diego

PUBLICATIONS

Parikh, P., Sina, M., Banerjee, A., Wang, X., D' Souza, M. S., Doux, J.-M., Wu, E. A., Trieu, O. Y., Gong, Y., Zhou, Q., Snyder, K. & Meng, Y. S. Role of Polyacrylic Acid (PAA) Binder on the Solid Electrolyte Interphase in Silicon Anodes. *Chem. Mater.* **31**, 2535–2544 (2019).

FIELDS OF STUDY

Major Field: Engineering

Studies in Materials Science and Engineering
Professor Ying Shirley Meng

ABSTRACT OF THE THESIS

Silicon and silicon oxide: Investigation of full cells, binder additive, and pre-lithiation for Li-ion batteries

by

Macwin Savio Dsouza

Master of Science in Materials Science and Engineering

University of California San Diego, 2019

Professor Ying Shirley Meng, Chair
Professor Ping Liu, Co-Chair

The advent of electric vehicles has uncovered the true potential for lithium-ion batteries (LIBs) however existing technology, can achieve a maximum energy

density of ~ 300 Wh/kg. In order to promote the global use of electric vehicles, it is necessary to achieve > 400 Wh/kg which can enhance the driving range and in turn lower the cost. Si-based alloy anode is a promising alternative compared to graphite, due to its higher specific capacity. However, severe volume change (> 300 %) during lithiation, currently hinders its commercial application. The effect of the volume expansion can be largely mitigated by efficient binder formulations and novel silicon oxide-based chemistries. However, the understanding must be translated into full-cell configurations also. In this work, first, the stability of the full cells is explored using Si anode coupled with NMC111 cathode. Our measurements indicate that capacity degradation is aggravated due to overcharging of the cathode. Preventive action to eliminate this overcharge rendered ~ 30 % increase in capacity retention. Second, to achieve improved coulombic efficiency (CE) > 99% and larger capacity retention, Ferritin, a protein, was incorporated as a binder additive. Attractive properties such as self-healing, flexibility, and rigidity which can sustain the structural integrity of the anode allowed for effective half-cell testing. Last, tackling the volume expansion was sought by use of silicon oxide (SiO_x) as the anode material. Pre-lithiation using stabilized lithium metal powder (SLMP) was also demonstrated to overcome low first cycle CE.

Chapter 1

Background

The modern world has become dependent on fossil fuels which are a finite source of energy. This extensive use of these depleting sources has resulted in an increase in the CO_2 emissions that is the primary reason for global warming. The realization of this effect has enabled the advent of electric vehicles and the push towards more renewable sources of energy. Battery technology has enabled the revolution of mobile phones, computers, and devices that have impacted the communication field. This technology raises some vital questions: Can this technology serve as a tool to fight global warming? Is it possible to integrate this technology into the automotive industry and still achieve comparable performance with that of the internal combustion engine? A rechargeable battery provides a potential solution to these questions.

Over the past few years, Lithium-ion batteries (LIB) have gathered applications ranging from mobile devices to electric vehicles. This has turned LIBs into most widely used secondary battery systems due to its high energy density, high operating voltages, low maintenance, and limited self-discharge [1–4]. The electrode materials that are currently used commercially have allowed the design of batteries with an energy density of ~300 Wh/kg as shown in Figure 1.1 [5].

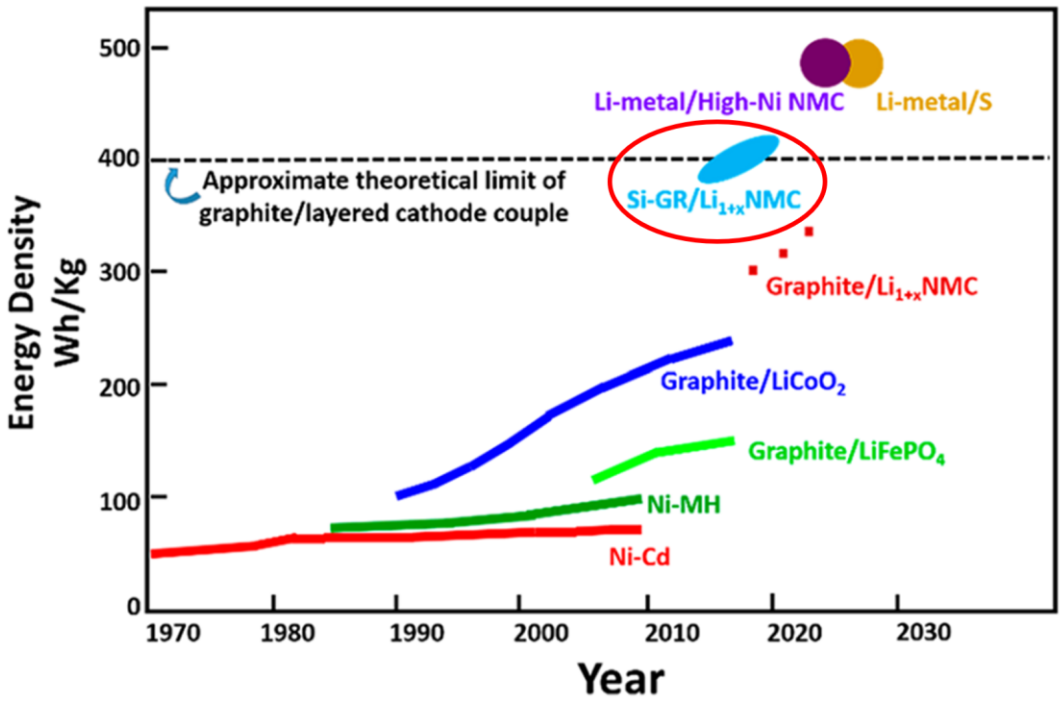

Figure 1.1. Evolution of energy densities for various battery chemistries. The red circle highlights the battery system with a Si anode. “Reprinted with permission [5]. Copyright 2018 American Chemical Society.”

Breaking this threshold of energy density is crucial to the deployment of electric vehicles around the globe. In many parts of the world, especially developing countries, electric vehicles are still in the development stage. A higher energy density will address the need for longer driving range for vehicles which can, in turn, reduce capital costs. Improvements in energy density can be achieved by three routes: 1) Decrease the total weight of the cell components, 2) Incorporating high-capacity electrode materials, 3) Increasing the operating voltage of the cell. This work focuses on enabling anode materials with higher capacity. Graphite, which is widely used as an anode material, has a specific capacity of 372 mAh/g [2]. Alternative

high-capacity anode materials such as Silicon (Si) can provide marginal improvement over current technology.

Si is one of the promising candidates to replace graphite anode due to following important reasons: (1) Si has a gravimetric energy density of 4200 mAh/g which is almost ten times higher than graphite. (2) Si is the second most abundant element on the earth which makes it a commercially viable material. All the techniques for manufacturing Si on a large scale have already been mastered due to its popularity in the semiconductor industry [6]. (3) The discharge voltage of Si is appropriate to avoid adverse Li plating while achieving reasonable open circuit potential [7].

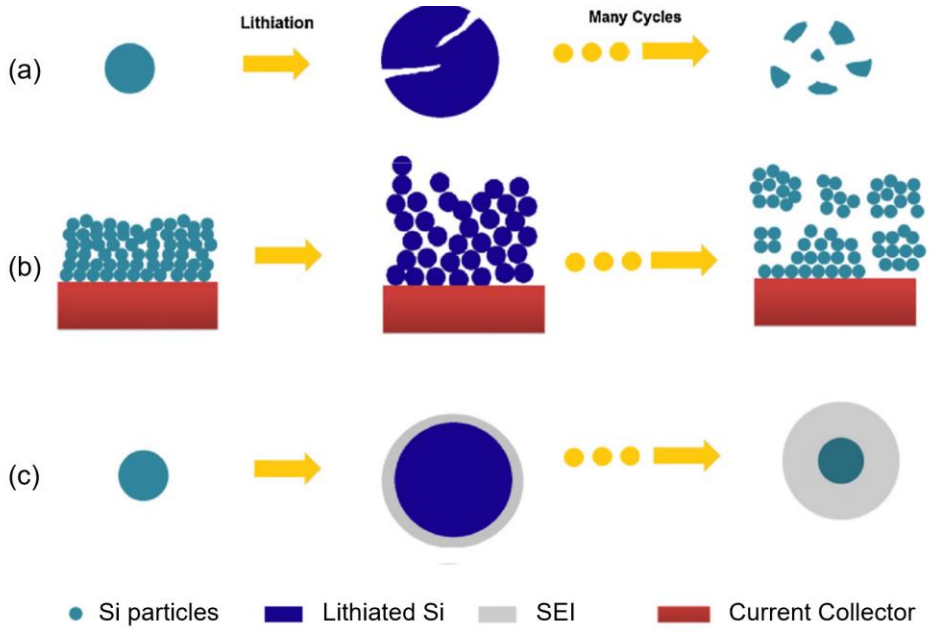

Figure 1.2. Failure mechanism of a silicon electrode, (a) pulverization of particles, (b) isolation of clusters of active material, and (c) continuous growth of SEI due to parasitic reactions. “Reprinted [6], Copyright 2012, with permission from Elsevier.”

However, the usage of Si as the active material is associated with limitations intrinsic to the material. Figure 1.2 shows the three failure mechanisms associated with Si when used in anode. When the cell is charged, lithiation (lithium ion insertion) of the electrode causes a drastic volume expansion of > 300 % and subsequent delithiation (lithium ion extraction) causes the material to contract. The immense stress leads to further consequences [6,8]. Pulverization and isolation of particles are observed on repeated cycling. Continuous breaking of particles exposes fresh active material surface to the electrolyte causing recurrent growth of the solid electrolyte interface (SEI) [9–11]. All the above processes consume Li ions leading to low coulombic efficiency (CE) and thus consuming the electrolyte. The result of this is drastic capacity loss and the electrode structure is deteriorated. To tackle these issues, researchers have identified different paths. All the research so far suggests that the performance of silicon electrodes depends on variety of factors such as particle size and shape, morphology, binder properties and additives, electrolyte and sacrificial additives, and electrode processing.

Formation of stable SEI has been studied by using sacrificial additives in the electrolyte [12]. Fluoroethylene carbonate (FEC) is an electrolyte additive which is shown to enhance the performance by forming thick and stable SEI components such as lithium fluoride [13]. Hence, FEC was chosen as the electrolyte additive of choice throughout this work. Additionally, many efforts have been made to overcome the limitations using novel Si materials. Some of them include using Si with different morphologies such as Si nanocrystals, Si nanowires, Si nanotubes,

and porous Si [14,15]. To avoid the issue of particle pulverization, nanocrystals of Si (~ 50 nm) are chosen in this work which have shown to not pulverize due to size effect [16]. **Chapter 2** presents the work on developing full cells using nanocrystalline Si as the anode material which leads to insights into a mechanism responsible for rapid degradation of performance in a full cell. NMC111 is used as the cathode material in this study. Furthermore, efficient binder systems have been developed to maintain the structural integrity of the electrode [17,18]. **Chapter 3** summarizes the advantage of using a protein-based binder additive, Ferritin, which can form reversible interactions in the anode. Preliminary results of electrochemical testing are presented. Also, silicon oxide (SiO_x) have been proposed to achieve better control over volume expansion [19]. **Chapter 4** discusses the pre-lithiation of SiO_x anode using stabilized lithium metal powder (SLMP) to boost the low 1st cycle coulombic efficiency associated with this material.

Chapter 2

Cathode Overcharge-Induced Degradation in Si-NMC111 Full Cells

2.1 Introduction

Si as the anode material has been under research for the last two decades and the focus has either been majorly on the materialistic design of Si or the auxiliary components such as binder, carbon, and electrolyte. However, most of the work on these systems is tested in a half cell configuration which is an efficient method to study the effects of a new system using Li metal as counter electrode. In order to ensure the commercial viability, it is necessary to study the electrochemical performance in a full cell configuration where the supply of cyclable Li is limited to that in the cathode. Three different methods are widely used to study full cells: Excess Cathode, Pre-cycling, and Pre-lithiation [20–23]. In the Excess Cathode full cells, excess capacity on the cathode side is considered to balance for the irreversible loss that occurs in the formation cycle of both the electrodes. Alternatively, the electrodes can be electrochemically cycled in a half cell for one cycle to mitigate the irreversibility before fabricating a full cell. This method is referred to as Pre-cycling. Pre-lithiation involves providing additional finite amount of Li^+ by internally shorting the Si anode with a Li source such as Li metal foil or stabilized lithium metal powder (SLMP) in order to take up the 1^{st} cycle loss [24]. This method will substitute the consumption of Li from the cathode and hence, improve the overall capacity.

In LIBs, two parameters are fixed before fabricating full cells: negative/positive (N/P) capacity ratio, and the cut-off voltage. These factors are dependent on the active materials of both the electrodes and the cycling conditions such as discharge current and operating temperature. The reversible capacities are prone to vary between electrodes. Hence, a reasonable adjustment of the mass of the active material is necessary. Specifically, N/P ratio of < 1 can promote chances of Li plating on the anode inducing safety concerns. On the other hand, N/P ratio of > 1 sacrifices the energy density of LIB due to presence of additional active material. In order to prevent safety issues while not sacrificing the energy density, an N/P ratio of ~ 1.1 to 1.2 is considered as an industry-standard where the anode is slightly oversized [25]. Additionally, as no reference electrode (RE) is utilized in a full cell, the capacities are indirectly controlled by setting a cut-off voltage. This is determined by taking the difference between the intended end potentials of charge/discharge for the electrodes. This cut-off voltage should be optimal to achieve the highest energy density.

The source of capacity in a full cell is the positive electrode which is NMC111 cathode in this work. Changes in reversible capacities at the anode and cathode during cycling continuously change the N/P ratio. Since Si is associated with recurrent irreversibility due to factors described in Figure 1.2, cyclable Li^+ is lost increasingly at the anode. This problem has detrimental effects in a full cell cycling which is the focus of this work. Consequently, If the N/P ratio in a full cell increases during cycling, the cathode could overcharge leading to a higher degree of

delithiation causing irreversible structural changes. Furthermore, oxidative decomposition of the electrolyte at the cathode increases at elevated potentials. A systematic investigation of the charge-end potentials of individual electrodes is sought to gain insights into these processes.

Before the start of this work, the choice of a binder for Si anode was decided based on previous results in literature. Many researchers have focused on studying the effect of binders like sodium carboxymethyl cellulose (CMC-Na) and polyacrylic acid (PAA) on the performance of Si anode. Using CMC-Na as a binder leads to acceptable stability of Si anode but suffers from severe mechanical degradation due to lower expansion capability. Furthermore, CMC-Na is proven to achieve good stability only with lower loading of Si active material in a composite electrode [18]. In order to target higher energy density, PAA binder is the front runner with excellent stability. It provides better cycling performance compared to CMC-Na due to much higher concentration of -COOH functional groups [26]. Due to these advantages, PAA was chosen as the binder for this work.

At the onset, slurry making was optimized to achieve stable electrochemical performance for Si anode. NMC111 was the cathode of choice due to its high capacity, thermal and structural stability, and rate capability [27,28]. Pre-cycling method was selected to fabricate the full cells. This ensured the mitigation of loss of cyclable Li to the formation cycle of both the electrodes. To study the behavior of individual electrodes in a full cell, the potential profiles of the cathode and anode were determined using a three-electrode cell where Li metal was used as a reference. It

was observed that the continuous capacity fade gave rise to overcharging behavior of the cathode. The insights from the three-electrode cell testing were then incorporated to enhance the capacity retention of a full cell.

2.2 Experimental Methods

2.2.1 Electrode Fabrication

Si nanoparticles (Alfa Aesar, ~ 50 nm) were used as the active material for the anode and the fabrication was done as follows: 50 wt% nano-Si powder, 25 wt% carbon black, and 25 wt% polyacrylic acid (PAA, Mv = 450,000, Sigma Aldrich) were mixed in water. PAA was dissolved in water beforehand where the concentration of the final solution was 6 wt %. Two types of carbon black were explored: Ketjenblack (Akzo Nobel: EC-600JD), and Super P (Timcal). The slurry, prepared using a Thinky mixer, was then coated on a Cu foil (rough surface) by using a doctor blade and dried at 80 ^{o}C overnight under vacuum to completely dry any solvent. The electrode sheet was cut into a disk and applied for the battery test. The mass of the Si active material on the electrodes obtained was approx. 0.5 mg/cm^2.

The positive electrode was prepared as follows: 80 wt% $LiNi_{1/3}Mn_{1/3}Co_{1/3}O_2$ (NMC111) powder (Toda), 10 wt% carbon black (Timcal) and 10 wt% polyvinylidene fluoride (PVDF) were mixed in N-methyl-2-pyrrolidone (NMP) as a solvent to prepare a slurry. The obtained slurry was coated on Al foil by using a doctor blade and dried at 80 ^{o}C overnight under vacuum to completely dry any solvent. The mass

of active material on the cathode was approx. 7.9 mg/cm^2. This mass varied based on the precise capacity obtained when electrochemically pre-lithiating the anode for full cells.

2.2.2 Electrochemical Testing

These electrodes were used to assemble coin cells, both half and full cells, using a polymer separator (C480, Celgard Inc.). The electrolyte (Battery grade, Gotion) was a solution of 1 M $LiPF_6$ dissolved in EC/DEC/FEC 45:45:10 (wt%). 100 µl electrolyte was used in fabricating both half and full cells. Li metal was used as the negative electrode when fabricating half cells. Three-electrode full cells (Swagelok) were assembled using Li metal as the reference electrode and glass fiber separators (Whatman). These cells were flooded with electrolyte in order to mitigate any pockets of Argon within the setup. All the cells were assembled in a glove box purged with high purity Argon gas and maintained at water vapor < 1 ppm.

Arbin battery cycler was used to electrochemically cycle the cells in the galvanostatic mode. The cells were rested for 10 hours after assembling while monitoring the open-circuit voltage (OCV) following which they were charged/discharged. The voltage window for NMC111 cathode is 3 V to 4.3 V, and Si anode is 1 V to 0.05 V. The formation cycle was carried out at a slower rate of C/20, and C/10 was used thereafter until 100 cycles. These rates are used while assuming a theoretical capacity of 200 mAh/g for the NMC111 cathode, and 3875 mAh/g for the Si anode. Hence, the actual rate of cycling can be higher based on the capacity delivered by the electrodes.

2.2.3 XRD and SEM

Coin cells were disassembled inside the Argon glovebox after completing 100 cycles of charge/discharge. The Si anode for analysis was always in the delithiated state, and NMC111 cathode was in the lithiated state. The electrodes were rinsed with DMC to remove any electrolyte residue on the surface and dried. Phase and crystallinity of the pristine and cycled NMC111 cathodes were determined by XRD at room temperature. The cathode films were removed from the Cu current collector and placed in a 0.5 mm diameter borosilicate capillary tube. The Mo Kα 2D PXRD capillary experiments were performed on Bruker APEX II Ultra diffractometer equipped with microfocus rotating anode operating at 50kV and 50mA power. X-ray beam was focused using Double Bounce Multilayer Mirror and divergence was controlled using 3mRad collimator. Diffraction images were collected at three different 2θ positions covering range to approx. 40° in 2θ. 2D diffraction images were reduced using DiffracEva V 4.3 (Bruker) software to standard RAW file format. The cross-section and surface micrographs of the Si anode were collected using a field emission scanning electron microscope (SEM, FEI Quanta).

2.3 Results and Discussion

2.3.1 Optimization of the Slurry

Electrode fabrication was initiated with the recipe for slurry making and casting explained in section 2.1.1. PAA was chosen as the binder of choice due to

well-documented stability in Si-based anodes [29,30]. Two types of carbon black were explored. When the slurry obtained with Ketjenblack (KB) carbon (Figure 2.1 (a)) was cast and dried, the electrode developed cracks. Figure 2.1 (b, c) shows large continuous cracks on the pristine electrode surface which were prevalent despite obtaining a consistent slurry. Dispersion of binder in different solvents like ethanol as well as variation of solvent concentration for the preparation of PAA solution resulted in cracks identical to that shown in Figure 2.1 (b, c).

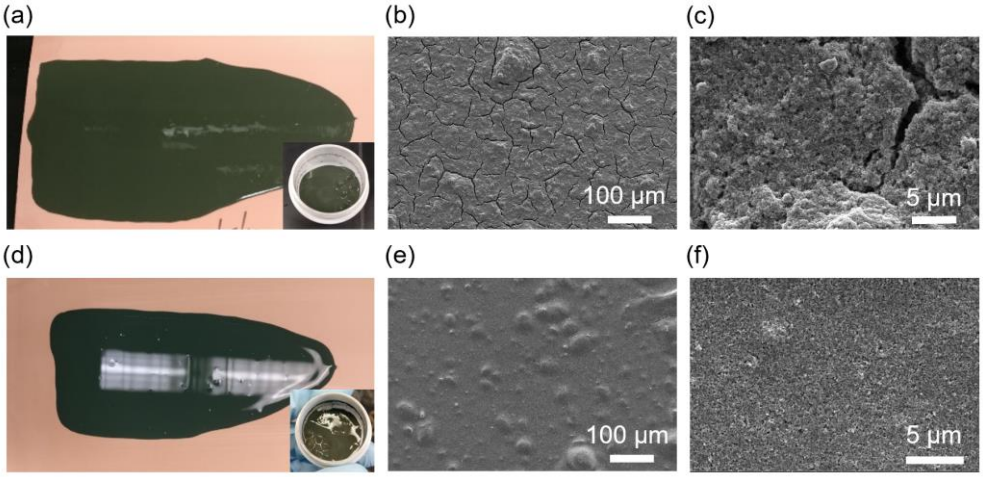

Figure 2.1. (a) Optical image, and (b, c) SEM of a film of a Si anode cast on the Cu foil with Ketjenblack carbon. (d, e, f) Corresponding images for a Si anode cast with Super P carbon. The insets in both (a) and (d) show the slurry after mixing in the Thinky mixer.

A new slurry was prepared and cast (Figure 2.1 (d)) by only varying the carbon type from KB to Super P. SEM of this newly fabricated electrode showed no signs of cracking (Figure 2.1 (e, f)). Since equivalent percent of carbon was being added to make the slurry, the much larger surface area in the case of KB (surface area of KB is 1400 m^2/g compared to 62 m^2/g of Super P [31,32]) may be utilizing most

of the binder resulting in excessive cracking of electrodes. Hence, the recipe with Super P carbon was chosen for all the subsequent testing.

2.3.2 Electrochemical Performance of Half Cells

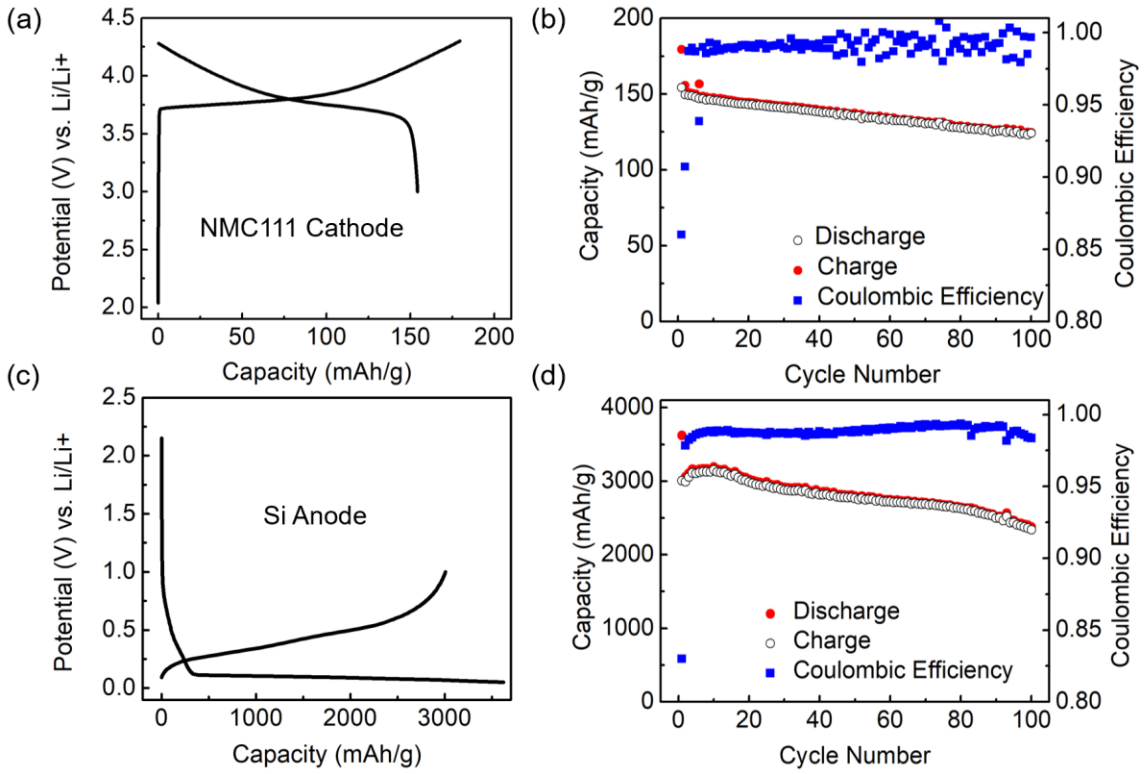

Figure 2.2. Voltage profiles for the 1st cycle for (a) NMC111 cathode, and (c) Si anode. Electrochemical performance for (b) NMC111 cathode, and (d) Si anode half cells for 100 cycles.

The electrodes were tested in a half cell configuration against Li metal as the counter electrode. Figure 2.2 (a, c) shows the first cycle voltage profile for Si anode and NMC111 cathode half cells. Si anode displays a discharge capacity of 3623 mAh/g and a charge capacity of 3007 mAh/g. The first cycle coulombic efficiency (CE) obtained is 82.99 % which is comparable to the recent work [33,34]. Additionally,

NMC111 cathode displays a charge capacity of 179 mAh/g and a discharge capacity of 154 mAh/g with the first cycle CE obtained is 86.00 %. The capacity retention and CE for the respective electrodes over 100 cycles are shown in Figure 2.2 (b, d). Both the half cells displayed excellent capacity retention, consequently, were reproduced and used in fabricating full cells.

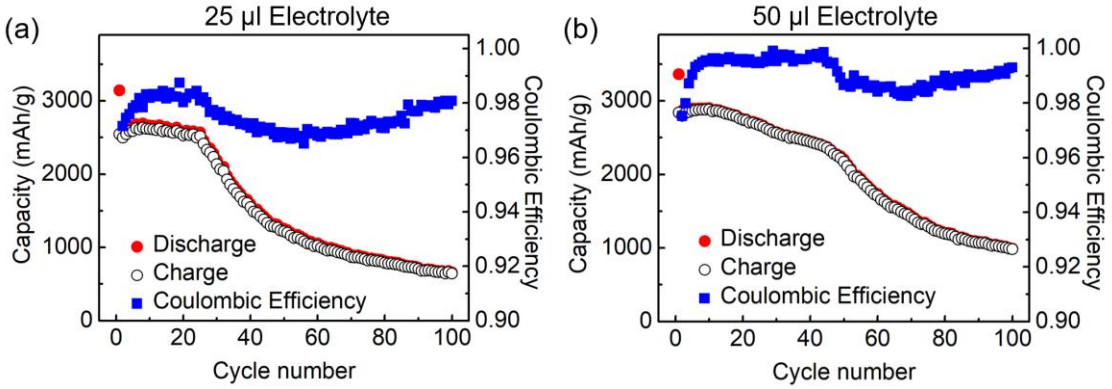

Figure 2.3. Electrochemical performance for Si anode half cells with PAA binder when electrolyte amount is controlled to (a) 25 µl, and (b) 50 µl.

The effect of electrolyte amount added when fabricating half cells was investigated for Si anode half cells. The half cell is shown in Figure 2.2 (c, d) was fabricated using 100 µl electrolyte which displays a stable performance over 100 cycles. As shown in Figure 1.2 (c), Si tends to suffer from continuous growth of SEI due to large volume expansion of the particles. This SEI on a Si anode comprises of products formed from electrolyte reduction which recurrently consumes the electrolyte [20]. To test this effect, half cells were constructed with 25 µl and 50 µl of electrolyte. It can be seen from Figure 2.3 (a), the cell with 25 µl undergoes a sudden failure at 26th cycle. This is due to the excessive consumption of electrolyte which

impedes the adequate diffusion of the Li ions between the two electrodes. The same effect can be seen with 50 µl at 45th cycle (Figure 2.3 (b)). In order to avoid the effect due to electrolyte consumption on the overall performance of a full cell, the amount of electrolyte in all the cells was fixed to 100 µl.

2.3.3 Preliminary Testing of Pre-cycling Full Cells

Pre-cycling method was chosen to fabricate full cells. In this method, the individual electrodes are electrochemically cycled for a cycle before assembling into a full cell. This method is advantageous where it prevents the loss of Li due to the formation of SEI which occurs in the first cycle. As shown in section 2.3.2, the first cycle CE for NMC111 cathode and Si anode are 86.00 % and 82.99 %. This CE will result in a remarkable loss of the finite Li if the electrodes are not pre-cycled.

After cycling the electrodes in a half cell for 1 cycle at C/20, the cells were disassembled inside the glove box purged with high purity Argon and the electrodes were put together into a full cell. Figure 2.4 (a) shows the components that are present in a full cell in a coin cell configuration. As Li is the species responsible for the capacity, a large amount of the irreversibility is presumed to be eliminated before assembling the full cell. Furthermore, 10% excess capacity is mandated for the anode to avoid the possibility of Li plating while cycling the cell [25]. Equation 2.1 is used for capacity matching of the full cell where Q_{rev} is the reversible capacity of the anode/cathode for the first cycle, m_A/m_C is the active material mass of the anode/cathode. The factor of 1.1 resembles a 10 % excess capacity on the anode.

$$1.1 \times Q_{rev}\left(\frac{mAh}{g}\right) \times m_A\left(\frac{mg}{cm^2}\right) = Q_{rev}\left(\frac{mAh}{g}\right) \times m_C\left(\frac{mg}{cm^2}\right) \qquad \text{Equation 2.1}$$

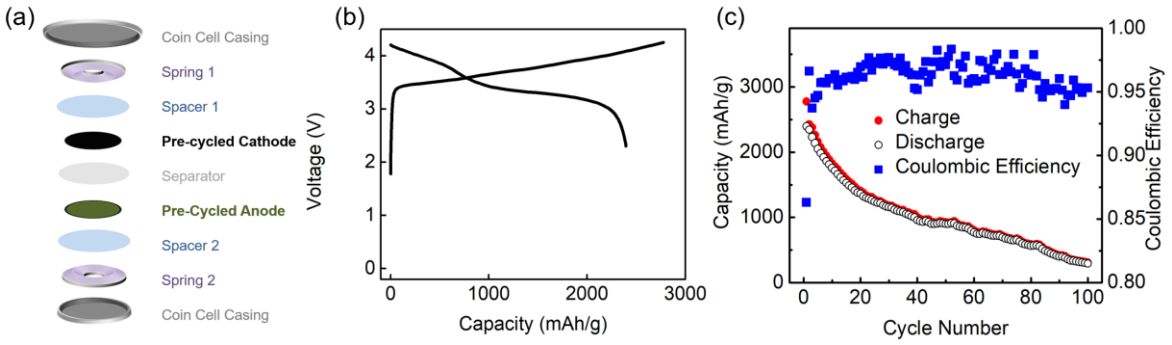

Figure 2.4. Schematic of all the components in a full cell made from 2032 coin-cell casing. The electrolyte added is not shown. (b) Voltage profile for the 1st cycle, and (c) electrochemical performance for a Pre-cycled full cell fabricated with an NMC111 cathode and a Si anode.

The full cell was cycled in a voltage window of 2.3 V to 4.25 V at a rate of C/10. This voltage window was chosen based on the redox plateau on the half cell potential profiles (Figure 2.2 (a, c)). Figure 2.4 (b) shows the voltage profile of the first cycle of the full cell. The first cycle has a charge capacity of 2776 mAh/g_{Si} and a discharge capacity of 2396 mAh/g_{Si}. The first cycle CE obtained is 86.29 % which could be due to the combined loss at the electrodes in the second cycle. The capacity continuously dropped causing complete failure after 100 cycles (Figure 2.4 (c)). The increasing variance in the CE after ~ 20 cycles is evidence of instability within the system which needs to be investigated.

2.3.4 Insights from Three-Electrode Cell Tests

Failure of a full cell can result from the capacity imbalance between the two electrodes. This imbalance causes the individual potentials of the electrodes to vary from the desired value when the same voltage is maintained. The kinetics of the materials involved also contribute to this problem [25] [23]. When a two-electrode system such as a coin cell is used, it is only possible to measure the voltage. A three-electrode cell must be fabricated in order to determine the potentials of individual electrodes.

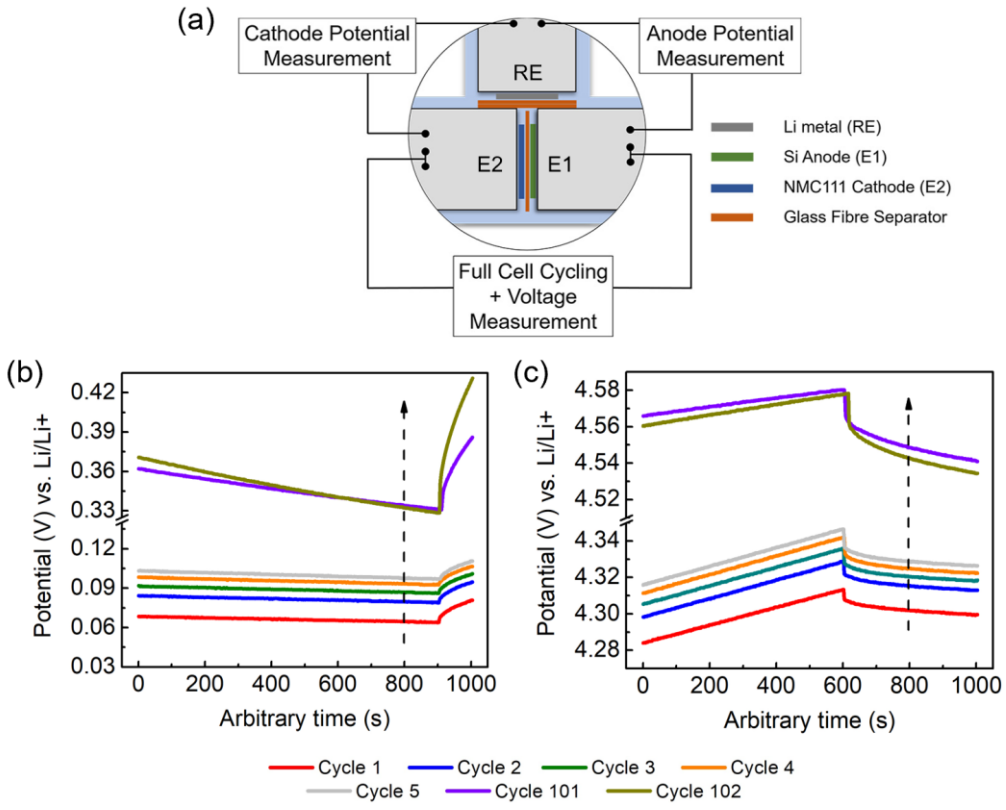

Figure 2.5. (a) Schematic of a three-electrode cell made of a Si anode (E1), and an NMC111 cathode (E2) with Li metal as a reference electrode (RE). End-of-charge potential profiles for (b) anode, and (c) cathode derived from the three-electrode cell.

A three-electrode cell was fabricated as shown in Figure 2.5 (a). Li metal was used as the reference electrode (RE). The electrodes were punched into 12 mm diameter discs and placed in contact with the plungers. A glass fiber separator was placed between the two electrodes. The space between the Li metal RE and the two plungers was increased by placing two glass fiber separators. This was done to prevent the effect of geometrical asymmetry, if present, on the stability of the potential at the RE surface [35,36]. The cell was cycled as usual between the NMC111 cathode and Si anode contacts. The RE contact was used to measure their potentials separately.

Table 2.1. Charge-end potentials of the anode and cathode determined form three-electrode measurements in a pre-cycled full cell.

Cycle Number	Anode Charge-End Potential (V) vs. Li/Li^+	Cathode Charge-End Potential (V) vs. Li/Li^+
1	0.0639	4.3134
2	0.0789	4.3287
3	0.0863	4.3358
4	0.0927	4.3419
5	0.0970	4.3466
101	0.3309	4.5803
102	0.3284	4.5784

The potential profiles at anode and cathode are plotted to show the portion in the vicinity of the charged state of the full cell Figure 2.5 (b, c). It is evident that

the charge-end potential of the anode and cathode increase continuously for the first five cycles. A three-electrode cell was assembled using the electrodes derived from a full cell cycled in a coin cell configuration. The charge-end potentials measured for both the electrodes after 100 cycles, shown in Table 2.1, increase to a much higher value where the NMC111 potential reaches ~4.58 V. This value is much higher than the intended limit of 4.3 V for NMC111 cathode.

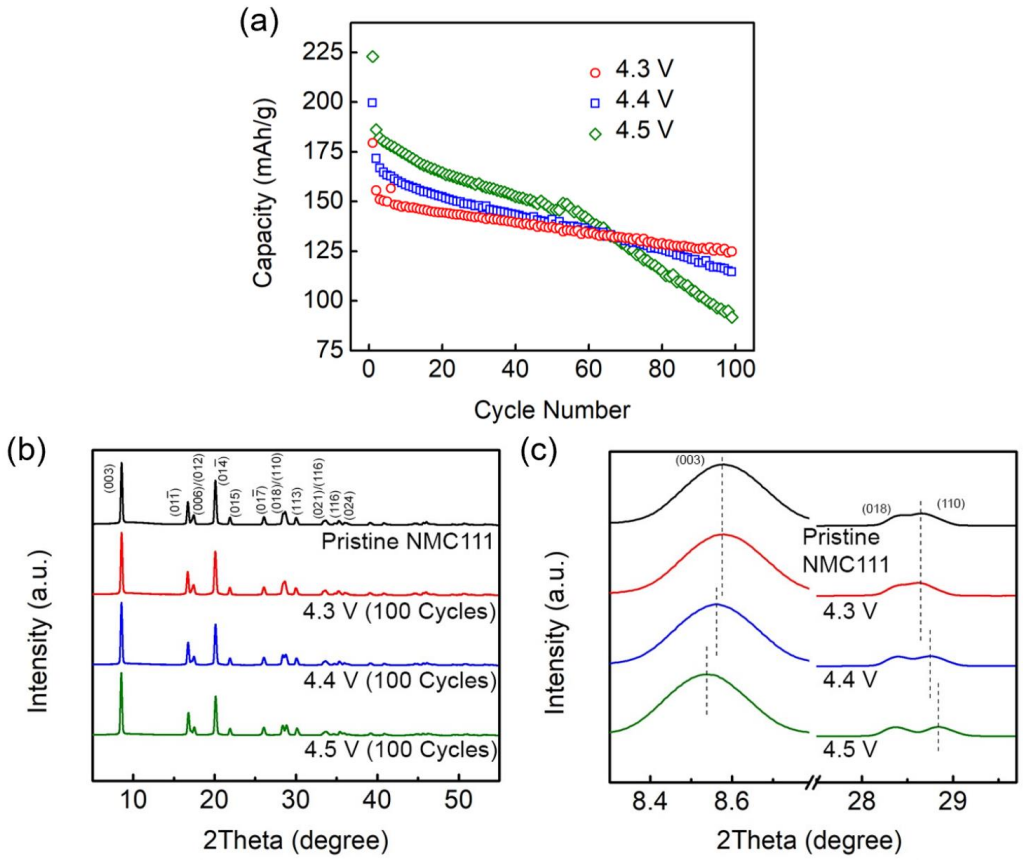

Figure 2.6. (a) Electrochemical performance comparison between NMC111 half cells cycled to charge potential cut-off of 4.3 V, 4.4 V, and 4.5 V. (b, c) XRD spectra for pristine NMC111 electrode compared to those cycled to charge potential cut-off of 4.3 V, 4.4 V, and 4.5 V for 100 cycles.

In a full cell, the cathode potential overcharge arises when the N/P is in excess of 1. In the current system, as the cycling progresses, the capacity degrades continuously (Figure 2.4 (c)). This capacity is equivalent to available Li in the NMC111 cathode for a full cell. As the available Li in the cathode decreases, the N/P ratio evidently increases causing overcharge of the cathode. Specifically, for NMC111 material, this overcharge can lead to CO_2 evolution starting at 4.3 V followed by O_2 evolution [37,38].

Electrochemical performance of NMC111 cathode was tested to understand the stability in different potential window cut-off of 4.3 V, 4.4 V, and 4.5 V in a half cell. It can be seen in Figure 2.6 (a) that increasing the cut-off deteriorates the capacity. This capacity loss may be due to the phase transformations occurring in NMC cathode at higher potentials. It is well known for NMCs that at higher potentials the layered structure undergoes transformation to spinel and rock salt phases which result in capacity fade due to the material loss in addition to increasing the interfacial resistance [39,40]. This phenomenon can be applied to the performance in Figure 2.6 (a). Due to the utilization of an infinite source of Li in half cell, the capacity can be regained in full if the above phenomena were absent.

To check the state of charge (SOC) of the cathode indirectly, XRD measurements were carried out to compare the structure and lattice parameters of post-cycled samples. It can be seen in Figure 2.6 (b, c) that (003) peak has a left shift to smaller 2θ, while (110) peak undergoes a right shift to higher 2θ. The lattice parameters were determined using Rietveld refinement which is presented in Table

2.2. Both Bragg factor (R_B) and weighted profile R-factor (R_{wp}) have values lower than 10 %. The 'a' lattice parameter decreases from 2.8640 Å to 2.8517 Å when the potential cut-off is increased. This may be due to the presence of smaller ions of transition metals due to change in oxidation state (e. g. Ni^{2+} to Ni^{3+}) [41]. Table 2.2 further confirms the increase in 'c' lattice parameter from 14.2474 Å to 14.3159 Å when the potential cut-off is increased. This may be caused by the increasing electrostatic repulsion between the MO_2 (M is $Ni_{1/3}Mn_{1/3}Co_{1/3}$) layers due to decrease in Li^+ ions between them [42].

Table 2.2. Lattice parameters of pristine, and cycled cathode particles.

Sample	a (Å)	c (Å)	R_B	R_{wp}
Pristine NMC111	2.8640	14.2474	0.8761	2.33
4.3 V (100 cycles)	2.8671	14.2454	1.052	2.73
4.4 V (100 cycles)	2.8588	14.2770	0.811	2.65
4.5 V (100 cycles)	2.8517	14.3159	0.8411	2.83

Hence, it can be concluded that increasing the potential cut-off degrades the cathode capacity extensively by factors that can be related to structural transformations or interfacial resistance within the material. This was further tested in a full cell.

2.3.5 Improvement in Performance of Full Cells

The cathode overcharge can lead to excessive degradation as shown in section 2.3.4. This hypothesis was tested in full cells by restricting the charge

voltage to lower values. By doing this, it is possible to prevent the cathode from exceeding its safe cycling window even if there is an occurrence of overcharge. The full cell fabricated in section 2.3.3 was cycled in a voltage window of 2.3 V to 4.25 V. Additional cells were tested when charged to 4.1 V and 4.0 V (Figure 2.7 (a, b)).

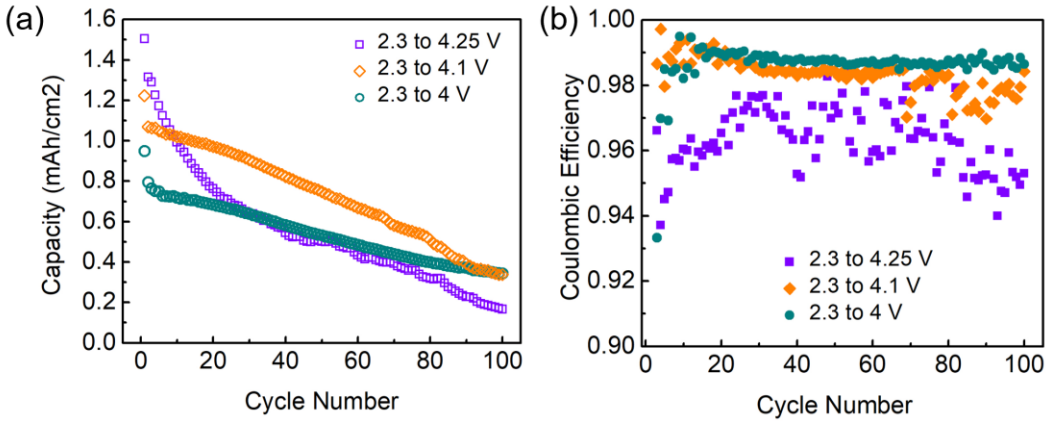

Figure 2.7. (a, b) Electrochemical performance comparison between Pre-cycled full cells cycled to charge potential cut-off of 4 V, 4.1 V, and 4.25 V for 100 cycles.

Table 2.3 presents the electrochemical testing results for three different protocols. When the charge cut-off was restricted to 4.0 V the retention in capacity was improved by ~30 %. This helped prove that the cathode overcharge is indeed contributing to the failure in a full cell. It is also vital to note from Figure 2.7 that lowering the cut-off increases the CE and its stability over 100 cycles. However, this method sacrifices the capacity that a cell can deliver, hence, this method is just a preventive measure. More alternatives to solve this problem will be discussed in subsequent section.

Table 2.3. Electrochemical testing results for full cells with charging cut-off of 4.25 V, 4.1 V, and 4.0 V.

	2^{nd} Cycle Charge Capacity (mAh/cm^2)	100^{th} Cycle Charge Capacity (mAh/cm^2)	Capacity Retention, Cycle 2 to 100 (%)
2.3 to 4.25 V	1.31522	0.16612	12.63059
2.3 to 4.1 V	1.06909	0.33737	31.55674
2.3 to 4.0 V	0.79385	0.34345	43.26384

2.3.6 Degradation Mechanism in a Full Cell with Si Anode

In a full cell, the capacity is limited to the amount of Li in the cathode. This loss of capacity leads to a recurrent increase in the N/P ratio above 1 which is responsible for potential overcharge at the cathode. An overcharged cathode can undergo structural transformations which contribute to the capacity fade. Figure 2.9 compares two cases where the charging cut-off is 4.25 V and 4.0 V. In the case of 4.25 V, the cathode potential transcends above the safety limit which accelerates the degradation of the full cell. However, in case of 4.0 V, the cathode potential stays within the safety limit. This can prevent perceived structural-induced degradation contribution. It is important to note from Figure 2.8 and Figure 2.7 (a) that the full cell undergoes degradation despite the control of voltage to 4.0 V. Hence, there may be other factors which need to be addressed to achieve a robust full cell.

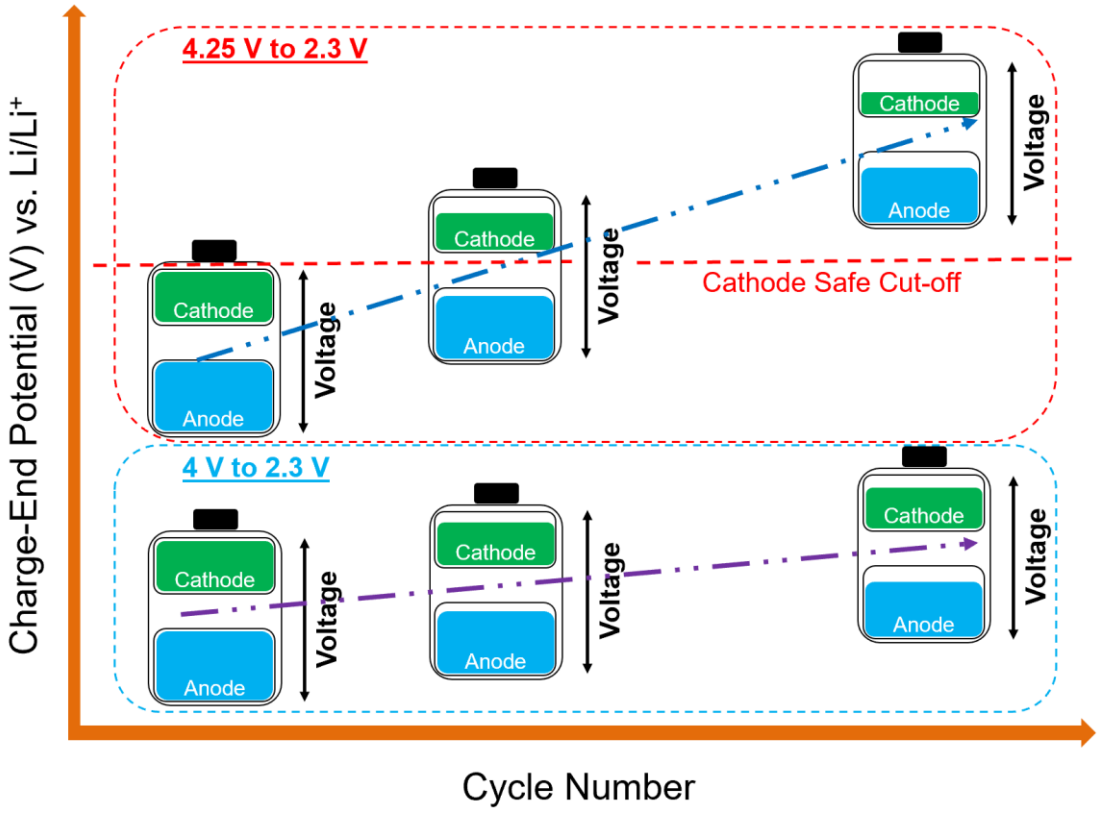

Figure 2.8. Schematic showing the degradation mechanism in a full cell caused by cathode overcharge. The horizontal red dotted line is the safe cut-off potential for a cathode.

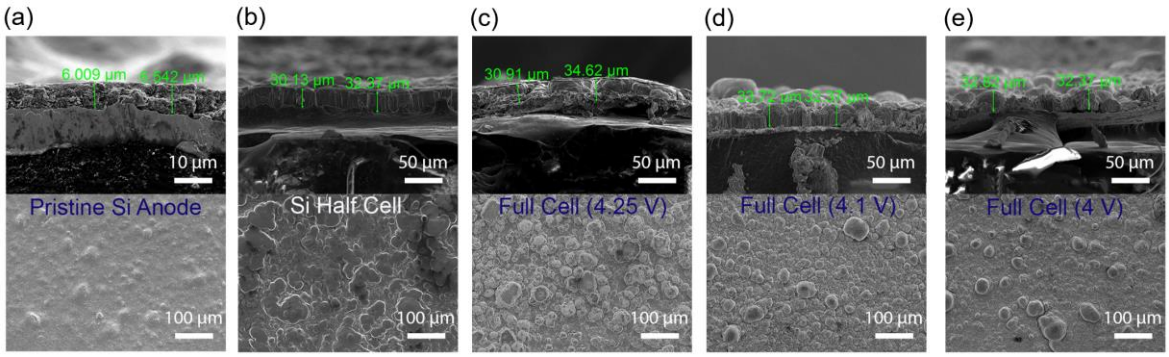

Figure 2.9. SEM cross-section (top) and morphology (bottom) for pristine Si anode (a) compared to anodes extracted from (b) half cell, and full cells cycled to charge potential cut-off of (c) 4 V, (d) 4.1 V, and (e) 4.25 V in full cells for 100 cycles.

The morphology and cross-section of Si anodes were studied using SEM for each case (Figure 2.9). The thickness of the electrode on the Cu foil increased from ~ 6 µm to > 30 µm. This increase was not only seen in the half cell but for all three full cell cases of 4.25 V, 4.1 V, and 4.0 V. Additionally, the surface of Si anode developed unique morphology with swollen particles in all cases. It can be qualitatively inferred from SEM that the degradation of Si anode in all cases is identical. Limiting the voltage does not mitigate the degradation factor due to anode itself which is the root cause. Hence, any improvements in the anode will alleviate the performance of the full cell.

2.4 Conclusion and Future Work

In this chapter, the degradation mechanism of a full cell with Si anode and NMC111 cathode is studied. Both the anode and cathode recipes were first optimized to mitigate cracking on the electrodes and achieve good electrochemical stability in half cells for 100 cycles before proceeding to make full cells. The 1st cycle CE for cathode and anode were 86.00 % and 82.99 %. Pre-cycling method was chosen to make full cells to prevent the loss of Li to the 1st cycle capacity loss. Three-electrode cell configuration helped to determine the overcharge in NMC111 cathode potential to ~ 4.58 V while it was intended to limit at 4.3 V. This effect is due to the continuous increase in N/P ratio above 1 while cyclable Li is lost at the Si anode. Through half cell testing and XRD of NMC111 cathode to higher potentials of up to 4.5 V, it was concluded that a higher potential is detrimental for the performance.

To test the applicability of cathode overcharge on full cells, the voltage cut-off was modified. Consequently, the capacity retention in a full cell enhanced by 30 % when the voltage cut-off was lowered from 4.25 V to 4.0 V.

Even though, modifying the cycling protocol to prevent the overcharge induced degradation rendered enhancement, this method is not a permanent solution. By improving the reversibility at the anode, i.e. CE, it is possible to enhance the full cell performance and mitigate overcharge at the cathode. Since NMC111 has a layered structure which acts as a solid solution, the lithiation/delithiation signifies a continuous slope (Figure 2.2 (a)). It is hypothesized that the problem of overcharge can be prevented by using a cathode which has a plateau such as $LiFePO_4$, or $LiNi_{0.5}Mn_{1.5}O_4$. Work is currently under progress to improve the performance of the full cell using the strategies described above.

Chapter 2 is coauthored with Dr. Pritesh Parikh, Dr. Abhik Banerjee, Osman Trieu, Yongbai Josh Gong, and Prof. Ying Shirley Meng. The thesis author is the primary author of this chapter.

Chapter 3

Exploiting the Interactions of Ferritin as a Binder Additive in Si Anode

3.1 Introduction

Electrical isolation of particles is one of three major problems that contribute to capacity loss in a Si anode (Figure 1.2 (b)) [6]. The problem originates due to > 300 % volume expansion which is inherent to the material and increases the cell resistance resulting in a rapid capacity fade. This issue has been dealt for several years by improving the binding agent in a Si anode. Polymer binders play an important role in sustaining the structural integrity of the electrode film. This is due to the combined effect of independent physical properties of the polymer such as functionality, polarity, viscosity, flexibility, and conductivity. Most popular polymer binders among those tested for Si anodes have been CMC, PAA, alginate, sugar-based polymers, polyimide, and conductive polymers have shown superior performance [18]. In general, polymer binders can be classified into three categories based on bonding strength and reversibility [26]:

1. Binders with weak interactions, such as van der Waals forces: These bonds rapidly dissociate under minimal mechanical stress but possess high reversibility. Although bond reversibility and strength are independent properties, the efficiency of bond reversibility in a Si anode depends directly on the strength. Hence, these bonds are incapable of recovery.

2. Binders with can undergo covalent crosslinking: Covalent bonds are strongest but fail to recover upon rupture. While the formation of a network through covalent crosslinking can improve the structural integrity, the irreversible nature of these bonds induces plastic deformation. Hence, causing electrode failure.

3. Binders with self-healing properties such as hydrogen bonding and ion-dipole interactions: This type of bond is weaker than a covalent bond but can form reversibly which is necessary as Si particles expand upon lithiation. The molecules which display this property can form interactions with each other and also with the silanol group which exists on the surface of the Si particle [18,26]. Hence, upon elimination of mechanical stress, the dissociated bonds recover owing to the high bond strength. This behavior is referred to as self-healing which is the capability to recover the binder-binder and binder-Si interactions after losing such interactions in the previous cycle due to the large volume expansion [26].

In general, increasing the bond strength is desirable to a certain threshold if reversibility can still be achieved. Polymers with weak interactions are not capable of sustaining the structural integrity of Si anode. On the other hand, covalent crosslinking provides strong interactions but fails to recover. Hence, interactions with self-healing property are ideal for Si anodes. A recent study focused on determining the effect of the structure-property relationship on cycling performance. They ranked the desired properties of binders for Si anode in the order: self-healing

> covalent crosslinking > stiffness > flexibility [43]. The self-healing property is shown to be most crucial for both higher capacity and cycling performance.

In order to achieve the desired properties, proteins were chosen as additives to the binder. Ferritin, shown in Figure 3.1 (a, b), is a human ferritin heavy chain (hFTN) made of 24 monomer protein subunits [44]. Each monomer unit, highlighted in red in Figure 3.1 (a), consists of numerous amino acids which are chained together through peptide bonds. Figure 3.1 (c) shows the formation of a peptide linkage. The properties that motivate the application of Ferritin in Si anode can be elucidated by its amino acid functional groups: 1) Histidine, Arginine, and Threonine contain hydrogen bond-forming moieties. 2) Asparagine, Lysine, Aspartate, and Glutamate contain moieties that can form ion-dipole interactions. 3) Asparagine, Lysine, and Glutamate can also provide flexibility due to their saturated groups. 4) Phenylalanine, Tyrosine, and Tryptophan contain functional groups with benzene rings which can provide stiffness. Ferritin may also aid in distributing the applied mechanical force to reduce the stress on each anchoring point. In polymer binders, branched-chain polymers have shown improved electrochemical performance. This is believed to be due to distribution of the mechanical stress applied on a single anchoring point through interchain cohesion [45].

Figure 3.1 (c) shows a hypothesized interaction of Ferritin with PAA in a Si anode where it forms ionic interactions as well as hydrogen bonds. When the anode is lithiated, individual Si particles expand. This causes some of the interactions between Ferritin and PAA to dissociate as the bonding sites on the particle move

farther apart. Upon delithiation of the anode, the Si particles contract to their original size. The dissociated hydrogen bonds then recover due to their high strength. Hence, these interactions will possibly ensure the reversibility of the anode to its original state and prevent capacity loss due to electrical isolation.

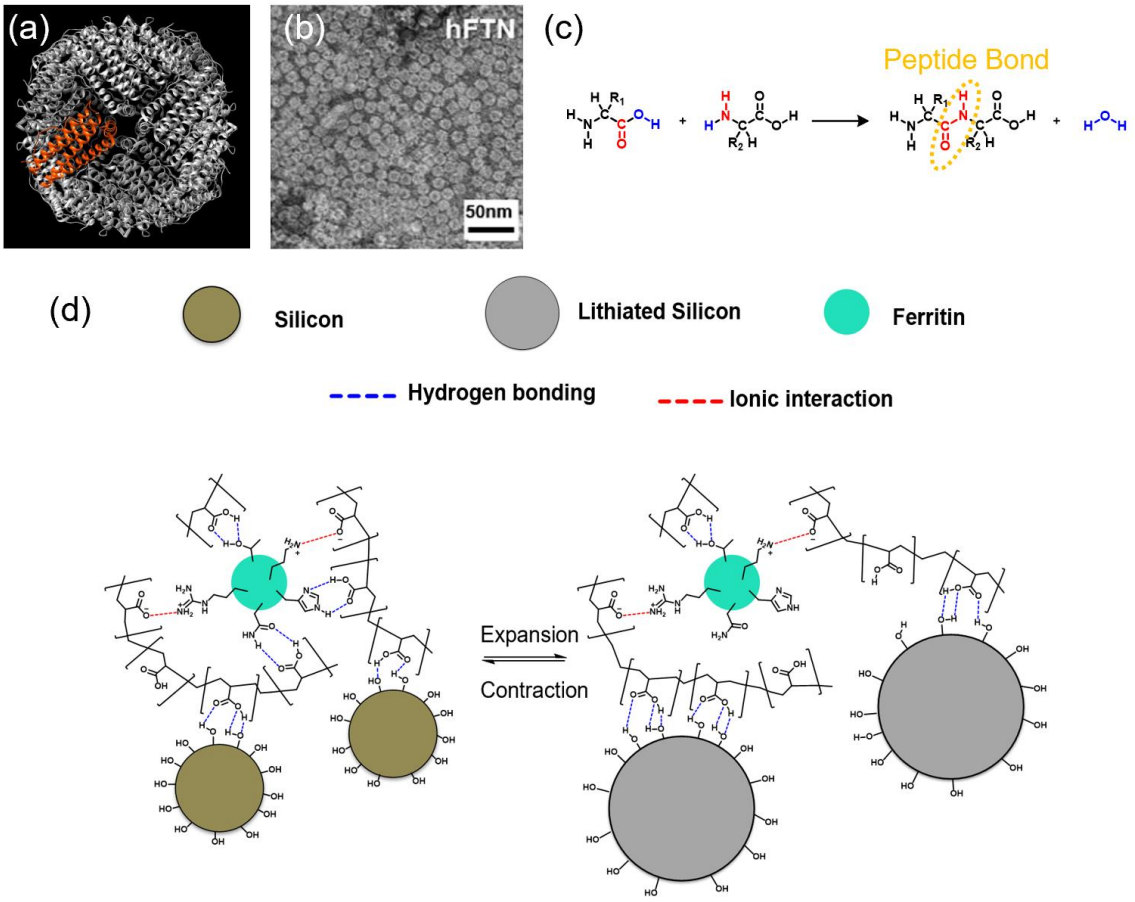

Figure 3.1. (a) Hollow ferritin molecule made of 24 monomer protein units. The red highlighted portion shows one such monomer unit. (b) Micrograph of human ferritin heavy chain (hFTN) dispersed on a TEM grid. “Reprinted with permission [46]. Copyright 2016 The Authors.” (c) Reaction between two amino acids to form a single molecule through a peptide bond. (d) Schematic showing the perceived interactions of ferritin with a PAA molecule when present in a Si anode.

Here, the project was initiated by studying the effect of Ferritin on the electrochemical performance of Si anodes. Ferritin, like every other protein, is sensitive to harsher conditions such as highly acidic/basic, high-temperature environment, etc., and can denature. The slurry process was modified to ensure Ferritin does not denature prior to cell testing. Electrochemical cycling was then conducted comparing the performance of cells with and without Ferritin.

3.2 Experimental Methods

3.2.1 Electrode Fabrication

The electrode fabrication was modified from section 2.2.1 to accommodate Ferritin into the system. The modified process is described below and the reasoning behind these steps is explained in detail in section 3.3.1. Si nanoparticles (Alfa Aesar, ~ 50 nm) were used as the active material for the anode and the fabrication was done as follows: 50 wt% nano-Si powder, 25 wt% Super P carbon (Timcal), and 25 wt% binder was mixed in water. PAA (Mv = 450,000, Sigma Aldrich) was dissolved in water beforehand where the concentration of the final solution was 5 wt %. LiOH salt was added to the 5 wt % PAA solution to obtain a pH in the range of 5 to 7. This final binder solution is henceforth referred to as Li-PAA. The slurry was then prepared using a Thinky mixer to which 20 µl of Ferritin (80 µM stock solution in water of hFTN) was added. It was then coated on a Cu foil (rough surface) by using a doctor blade and dried at room temperature for more than 30 hours under

vacuum to completely dry any solvent. The electrode sheet was cut into a disk and applied for the battery test. The mass of the Si active material on the electrodes obtained was approx. 0.5 mg/cm^2.

3.2.2 Electrochemical Testing

These electrodes were used to assemble half cells in coin cell configuration using a polymer separator (C480, Celgard Inc.). The electrolyte (Battery grade, Gotion) was a solution of 1 M $LiPF_6$ dissolved in EC/DEC/FEC 45:45:10 (wt%). 150 µl electrolyte was added and Li metal was placed as the negative electrode when fabricating half cells. All the cells were assembled in a glove box purged with high purity Argon gas and maintained at water vapor < 1 ppm.

Arbin battery cycler was used to electrochemically cycle the cells in the galvanostatic mode. The cells were rested for 10 hours after assembling while monitoring the open-circuit voltage (OCV) following which they were charged/discharged. The voltage window for Si anode is 1 V to 0.05 V. The formation cycle was carried out at a slower rate of C/20, and C/10 was used thereafter until 100 cycles. These rates are used while assuming a theoretical capacity of 3875 mAh/g for the Si anode. Hence, the actual rate of cycling can be higher based on the capacity delivered by the electrodes.

3.2.3 SEM

The surface micrographs of the Si anode were collected using a field emission scanning electron microscope (SEM, FEI Quanta).

3.3 Results and Discussion

3.3.1 Modification of the Slurry Process

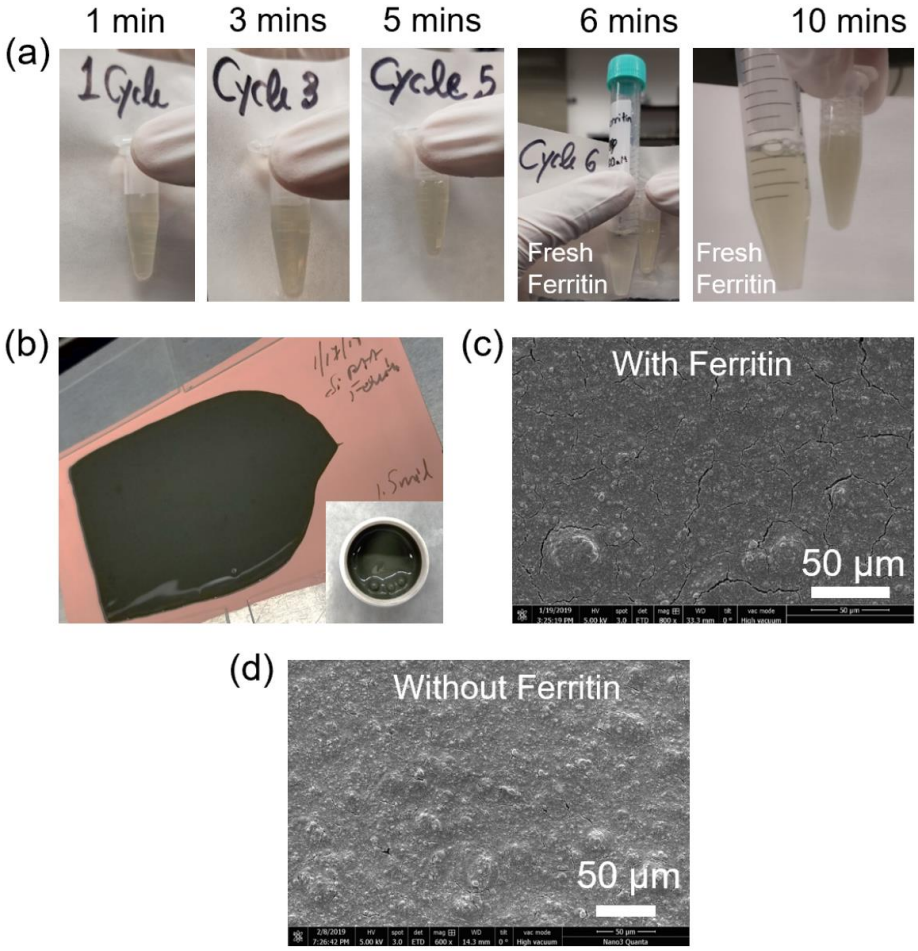

Figure 3.2. (a) Images showing the ferritin solution at specific intervals after mixing in a Thinky mixer with 3 balls. (b) Optical image, and (c) SEM of a film of a Si anode cast on the Cu foil with ferritin. The inset in (b) shows the slurry after mixing in the Thinky mixer. (d) SEM of the corresponding electrode without ferritin. The scale in (c, d) is 50 µm, however, the actual dimension is not equivalent as shown in the specifications bar at the bottom of the micrographs.

Ferritin, like any other biomolecule, is sensitive to its environment and can denature as a result. Denaturing is when the 24 monomers that makeup Ferritin

unfold to form agglomerations [44,47]. In the denatured state, Ferritin is no longer a spherical ball but instead dangling chains of protein monomers. This phenomenon can be easily identified as the solution containing the protein generally turns cloudy. For example, albumin which is present in an egg white turns opaque when boiled. Hence, it is crucial to address this sensitivity when incorporating Ferritin into a Si anode.

The properties of surroundings that are most sensitive to Ferritin are pH, and temperature [47]. In order to safely process the protein, each step in the slurry making process was evaluated and three major modifications were proposed. The following changes were made to the recipe described in section 2.2.1:

1. Ferritin is sensitive to pH in that it denatures in a strongly acidic or basic condition. PAA binder solution used in Si anode has a pH of 2 to 3 [34]. By neutralizing PAA solution using LiOH salt, a pH which is conducive for Ferritin was achieved (pH = 5-7). Hence, Li-PAA was chosen as the binder of choice for this system.

2. Friction and associated heat during mixing the slurry in a Thinky mixer could denature Ferritin [48]. The recipe involved mixing for 10 minutes which was found to achieve a homogeneous slurry. A Ferritin solution was mixed by itself in the Thinky mixer for 10 minutes with 3 balls to check the stability. It can be seen in Figure 3.2 (a) that Ferritin denatures after just 10 cycles of mixing. The safe limit is found to be 5 cycles after which the solution showed

signs of cloudiness. Hence, Ferritin is added to the slurry after some preliminary mixing of the other components such as Si composite and Li-PAA binder.

3. The vacuum drying of the slurry is usually done at 80 °C to eliminate any trace of water in the cast. However, Ferritin is stable below ~70 °C under atmospheric pressure [44]. To prevent the heat derived denaturing of Ferritin, this step was modified to a prolonged room-temperature vacuum drying for > 30 hours.

Figure 3.2 (b) shows the viscous slurry and a smooth cast obtained after the changes were incorporated. SEM of the electrode with Ferritin showed signs of minor cracking (Figure 3.2 (c)). Attempts were made to mitigate the cracks by varying the viscosity of the slurry but there was no effect on the result. Electrodes were prepared without the use of Ferritin to compare the morphology. Consequently, the cracks were seen also in the case of without Ferritin (Figure 3.2 (d)). It was concluded that the cracks could be characteristic of the Li-PAA binder and not inherent to Ferritin. Hence, electrochemical testing was conducted on the so obtained electrodes.

3.3.2 Improvement in Electrochemical Performance

The first cycle voltage profiles are identical for both with/without Ferritin trials. Figure 3.3 (b) shows the lithiation plateau from the highlighted region in Figure 3.3

(a). The plateau for both the cells with Ferritin is at a lower potential vs. Li/Li^+ than its counterparts. It can be inferred that the presence of Ferritin could increase the impedance of the cells which is responsible for lower capacities.

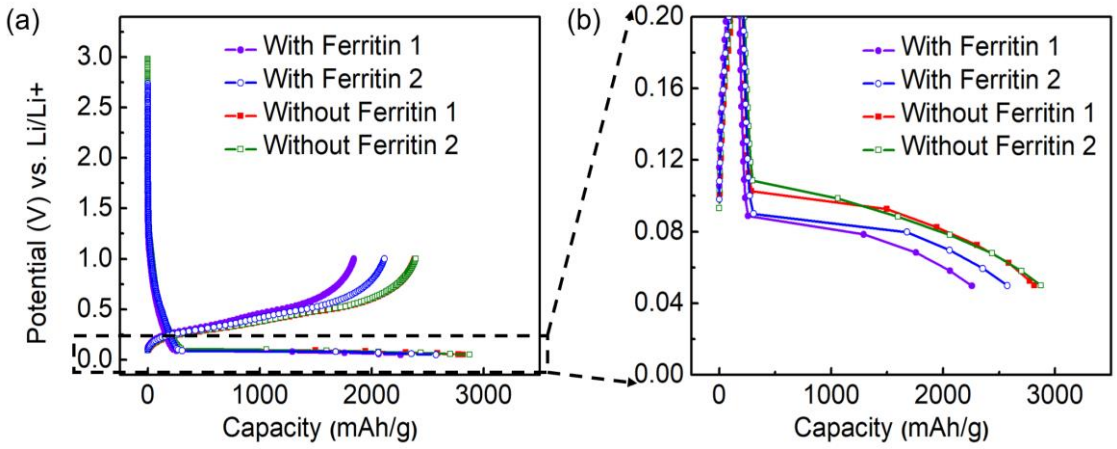

Figure 3.3. (a) Voltage profiles for the 1st cycle for Si anode half cells with and without ferritin. (b) Highlighted portion in (a) comparing the lithiation plateau of Si anode.

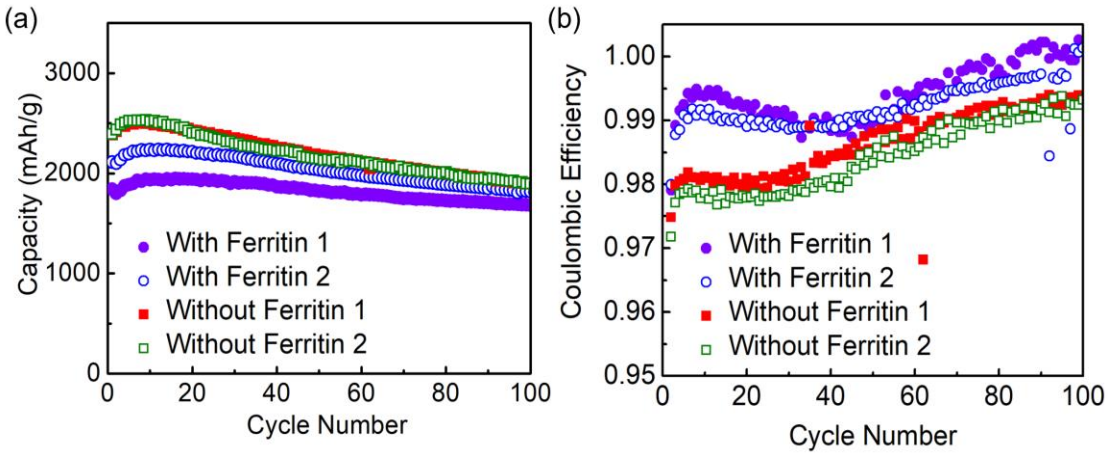

Figure 3.4. (a, b) Electrochemical performance comparison between Si anode half cells with and without ferritin.

Table 3.1. Comparison of electrochemical testing results for Si anode half cells with and without Ferritin.

	1st Cycle Charge Capacity (mAh/g)	100th Cycle Charge Capacity (mAh/g)	Capacity Retention, Cycle 1 to 100 (%)	1st cycle CE (%)	Average CE, Cycle 2 to 100 (%)
With Ferritin 1	1841.5586	1681.5094	91.31	81.60	99.41
With Ferritin 2	2112.4538	1816.5602	85.99	82.08	99.22
Without Ferritin 1	2386.1180	1896.2139	79.47	84.72	98.62
Without Ferritin 2	2393.2496	1896.5000	79.24	83.26	98.42

The electrochemical stability was monitored for 100 cycles (Figure 3.4). Table 3.1 provides a summary of the results for the same set of cells. The capacity retention for the cells with Ferritin is clearly higher which could be due to the higher CE. The reversibility is reflected by the average CE for Ferritin cells which is also higher than for the cells without Ferritin. However, the first cycle CE for the cells with Ferritin is lower which opens possibilities of electrochemical activity of the protein which is the subject of further investigation.

3.4 Conclusion and Future Work

In this chapter, Ferritin was used as an additive which can provide additional properties such as self-healing, rigidity, and flexibility to the binder. These properties are made possible through a variety of amino acid functional groups that make up

the protein. It was hypothesized that these properties could holistically improve capacity retention by alleviating the issue of electrical isolation in the Si anode.

At the onset of the work, modifications were made to the slurry process to accommodate the sensitivity of Ferritin toward harsher conditions of pH and temperature. The binder solution was neutralized to form Li-PAA. Mixing protocol and the drying step were altered to prevent friction and heat-related denaturing of Ferritin. When the electrodes were tested, it showed a clear improvement in capacity retention by at least ~ 6 %. The CE also saw an improvement.

However, the first cycle CE was lower for cells with Ferritin which implied that the protein additive could be electrochemically active. The electrochemical investigation of the protein is in progress. In addition, the applicability of Ferritin towards thick electrode and Micro-Si needs to be conducted which will be a beneficial strategy toward industrial viability. Finally, the interactions of Ferritin with Li-PAA and Si particles that are responsible for the improvement requires thorough investigation.

Chapter 3 is coauthored with Kenneth Han, Dr. Dijo Damien, Dr. Pritesh Parikh, Dr. Abhik Banerjee, Osman Trieu, and Prof. Ying Shirley Meng. The thesis author is the primary author of this chapter.

Chapter 4

Tackling the Low Initial CE in SiO_x by Pre-lithiation Using SLMP

4.1 Introduction

Si as the anode material has promising advantages but fails to provide the stability due to the large volume expansion of > 300 %. This is due to the recurrent formation of SEI, particle isolation, and pulverization of the particles [6]. However, the possibility of rendering a higher energy density has interested researchers to explore alternatives to harness the characteristics of Si.

Silicon oxide (SiO_x, x = O/Si atomic ratio) is a next-generation anode material that can provide a stable reversible capacity of 600 mAh/g [19,49]. This capacity is much lower than the theoretical capacity of Si (4200 mAh/g) but is higher than graphite (372 mAh/g). Hence, it can increase the energy density of the current technology. The lower capacity of SiO_x also addresses the problem of high-volume change during lithiation/delithiation which can potentially prevent capacity decay due to material loss.

SiO_x has many advantages but suffers from low (~ 50 %) initial CE [50]. This has been attributed to the formation of stable silicate and oxide phases (Li_4SiO_4 and Li_2O) due to the presence of excess O in the system [19,51]. These products formed are irreversible and lead to drastic capacity loss. In a full cell where the supply of Li is finite, it would be a detrimental loss of cyclable Li in the first cycle. This is a major

obstacle to overcome for commercial application of high-capacity anode material such as SiO_x.

A technique which is widely used to supply additional Li ions to address the issue of irreversible capacity is pre-lithiation. There are several methods for pre-lithiation: 1) electrochemically lithiating (vs. Li) the electrode in a half-cell. This method needs assembly and subsequent disassembly of half cells to utilize the electrode in a full cell which makes it commercially non-applicable [52]. 2) Chemical lithiation of the electrode using n-butyl lithium which is a hazardous chemical [53]. A third method which averts the limitations of both electrochemical and chemical method is pre-lithiation using stabilized lithium metal powder (SLMP). This method also referred to as internal short circuit, is a controllable way of lithiation. The SLMP is directly deposited on the electrodes and does not require any rearrangement or special structural requirement of the electrodes. This reduces assembly time and manufacturing costs, the factors which make it easy to integrate into existing industrial process. The method has been widely applied to graphite and Si anode where the first cycle CE was increased by 10 to 40 % [24,54–57].

Each particle of SLMP consists of 97 % Li coated with a thin layer of Li_2CO_3 [58]. Hence, it provides an alternative source of Li for the perceived irreversibility. The Li in the SLMP spontaneously reacts with Si through Equation 4.1 [55].

$$Si + xLi \rightarrow Li_xSi \left(\Delta G = -42 \frac{kJ}{mol}\right) \qquad \text{Equation 4.1}$$

In the presence of an electrolyte, reduction of the salt and solvent is initiated after the anode attains as OCV below the onset potential of SEI formation (~ 0.75 V vs. Li/Li^+ for SiO_x), depositing the thin passivation layer on the anode. The Li from SLMP also ionizes immediately after the injection of the electrolyte and electrons are released which move into the bulk of the anode. The Li^+ ions undergo solvation due to the presence of solvent molecules in the electrolyte. Lithiation of the anode starts thereafter when these solvated Li^+ ions undergo reduction consuming the electrons. The formation of a thin SEI layer and the Li_xSi alloy phase has been observed in Si anode through TEM of the pre-lithiated Si nanowires [55]. Hence, this method is a viable technique to enhance the reversible capacity of SiO_x by prematurely forming SEI and could react to form Li_4SiO_4 and Li_2O phases.

Recently, the pre-lithiation strategy has been applied to SiO_x in various forms which enhanced the CE > 80 %: 1) in situ mechanochemical reduction of SiO_x and Li metal [59], 2) Li powder-coated SiO_x electrode [60], and 3) double layer anode of SiO_x and Li layers [61]. SLMP has also been tested on SiO_x but the pressure was applied by rolling compression [62]. This work attempts to apply the strategy of SLMP pre-lithiation and also study the effect of pressure on the first cycle CE which has not been reported before. Here, SiO_x was first characterized to determine the properties such as morphology, and crystallinity of the material. It was subsequently tested to check the electrochemical stability. SLMP pre-lithiation was then applied to enhance the first cycle CE of the anode. Pressure activation by using a higher pressure is seen to enhance the reaction between SLMP and SiO_x anode.

4.2 Experimental Methods

4.2.1 Electrode Fabrication

SiO_x (SC, IFM Korea) was used as the active material for the anode and the fabrication was done as follows: 80 wt% SiO_x powder, 10 wt% Ketjenblack (Akzo Nobel: EC-600JD), and 10 wt% sodium carboxymethyl cellulose (CMC-Na, Mw = 250,000, Sigma Aldrich) were mixed in water. CMC-Na was dissolved in water beforehand where the concentration of the final solution was 3.2 wt %. The slurry, prepared using a Thinky mixer, was then coated on a Cu foil (rough surface) by using a doctor blade and dried at 80 ^oC overnight under vacuum to completely dry any solvent. The electrode sheet was cut into a disk and applied for the battery test. The mass of the SiO_x active material on the electrodes obtained was approx. 2 mg/cm^2.

4.2.2 Pre-lithiation using SLMP

A solution of 3 ml toluene (≥ 99.9 %, Sigma Aldrich) and 25 µl oleic acid (≥ 99 %, Sigma Aldrich) was prepared and stirred at 1000 rpm. 0.1347 g (~ 5 wt%) of SLMP powder (FMC Lithium) was added to the solution. The SLMP particles rise to the top of the solution due to the lower density of Li (0.53 g/ml) compared to toluene (0.87 g/ml). Hence, the solution was continued to stir at 1000 rpm throughout the process.

A SiO_x electrode is then placed in a coin cell can and the SLMP solution is dropped on the electrode using a micropipette. The solution is pipetted out in

samples of 10 µl to prevent overflow. Toluene on the electrode evaporates in a few minutes. A stainless-steel disk (~ 0.5 mm thickness) is placed on top of the electrode which is then pressed at 100 psi for 45 seconds using a regular coin cell crimping machine. The pressing ensures that the SLMP spherical particles are compressed and may also aid in breaking of the Li_2CO_3 shell on the particles [58]. Hence, increase the surface area of reaction. The whole process was carried out in a glove box purged with high purity Argon gas and maintained at water vapor < 1 ppm. The pre-lithiated electrodes are then processed to fabricate coin cells.

4.2.3 Electrochemical Testing

The electrodes were used to assemble half cells in coin cell configuration using a polymer separator (C480, Celgard Inc.). The electrolyte (Battery grade, Gotion) was a solution of 1 M $LiPF_6$ dissolved in EC/DEC/FEC 45:45:10 (wt%). 150 µl electrolyte was added and Li metal was placed as the negative electrode when fabricating half cells. All the cells were assembled in a glove box purged with high purity Argon gas and maintained at water vapor < 1 ppm.

Arbin battery cycler was used to electrochemically cycle the cells in the galvanostatic mode. The SiO_x cells were rested for 10 hours while the pre-lithiated cells were rested for 20 hours following which they were charged/discharged. A rest time of 20 hours has been identified as adequate for the reaction between SLMP and Si [56]. The voltage window for SiO_x anode is 2 V to 0.005 V. The formation cycle was carried out at a slower rate of C/20, and C/10 was used thereafter until 100

cycles. These rates are used while assuming a theoretical capacity of 1000 mAh/g for the SiO_x anode. Hence, the actual rate of cycling can vary based on the capacity delivered by the electrodes.

4.2.4 XRD and SEM/EDS

Phase and crystallinity of the pristine SiO_x powder were determined by XRD (Rigaku SmartLab) at room temperature. The powder was dispersed on a glass holder for measurement. Diffraction patterns were recorded using Cu Kα radiation over the 2θ range of $10° \leq 2\theta \leq 80°$ in Bragg-Brentano geometry. The surface micrographs and elemental distribution in the SiO_x powder were collected using a field emission scanning electron microscope (SEM, FEI Quanta).

4.3 Results and Discussion

4.3.1 Characterization of Pristine SiO_x powder

SEM/EDS was conducted to check the morphology and elemental distribution of SiO_x powder before proceeding for electrochemical testing. It was observed that the pristine SiO_x powder was a non-uniform distribution of particles forming agglomerates of ~ 20 µm (Figure 4.1 (a, b)). A surface elemental distribution using SEM/EDS shows the distribution of Si, C, and O across the powder (Figure 4.1 (c)). The O/Si atomic ratio obtained from EDS is ~ 1.4. It was found that 10 weight % C was added to potentially enhance the electronic conductivity of the powders. XRD was conducted to check the phase and crystallinity of the sample. It

can be seen in Figure 4.2 that the diffraction pattern is a diffuse peak between 15° ≤ 2θ ≤ 30° which is resonant with that of amorphous SiO [51].

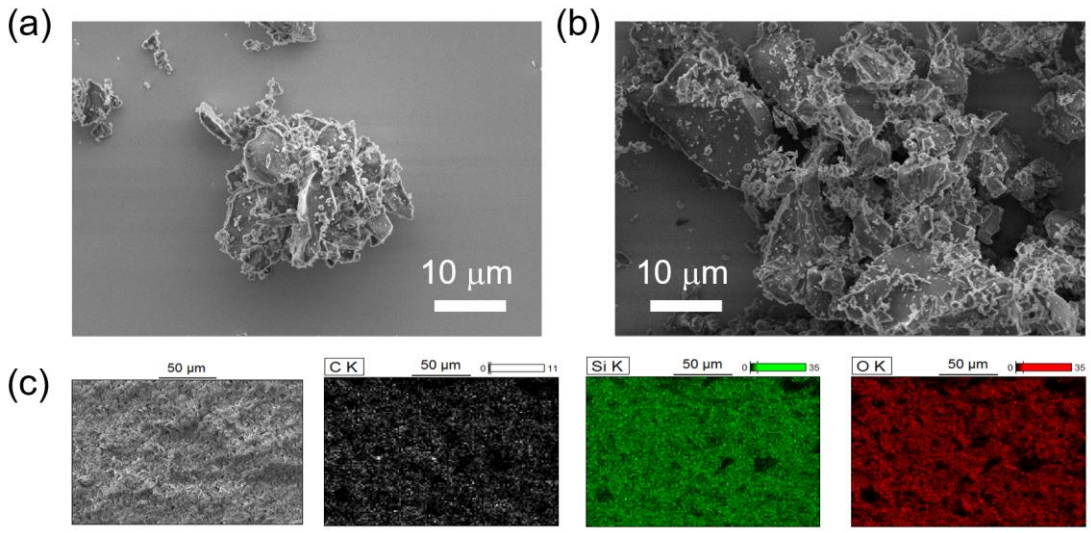

Figure 4.1. (a, b) SEM of SiO_x particles. (c) EDX of the particles shows the distribution of C, Si, and O elements.

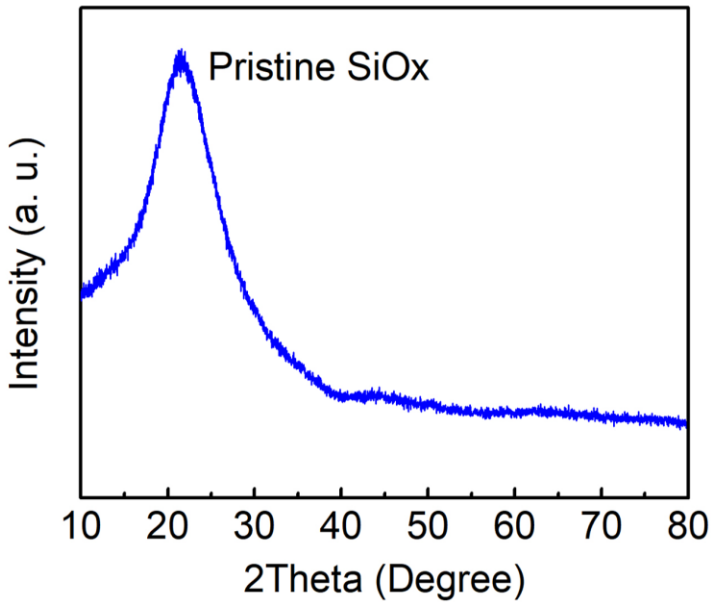

Figure 4.2. XRD of the SiO_x powder.

4.3.2 Preliminary Testing of SiO_x Anode Half Cells

The SiO_x powder was processed to make a slurry and half cells were fabricated to check the electrochemical performance (Figure 4.3). SiO_x anode displays a discharge capacity of 1372 mAh/g and a charge capacity of 686 mAh/g for the first cycle. The half cell showed excellent capacity retention of 94.81 % from cycle 2 to 100.

This stability is reflected by the CE trend which is ~1 after 50 cycles. However, as seen in Figure 4.2 (a), this material suffers from large irreversibility in the first cycle with a CE of 49.99 %. This is due to the inherent presence of high O content in the material which forms irreversible products such as Li_4SiO_4, and Li_2O during the initial cycles [51]. Efforts to tackle this issue trough pre-lithiation technique is presented in the following section.

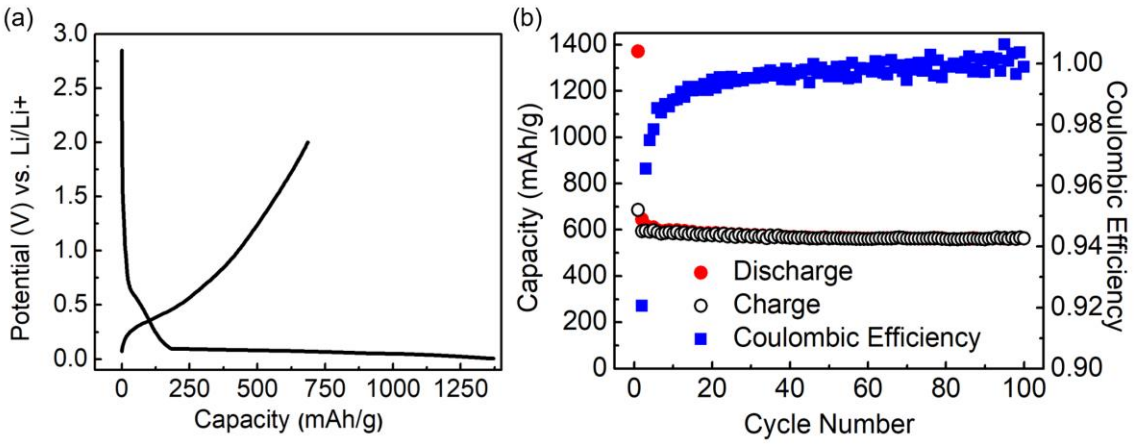

Figure 4.3. (a) Voltage profile for the 1st cycle, and (b) electrochemical performance for a SiO_x anode half cell.

4.3.3 Improvement in CE after Pre-lithiation

The electrodes were pre-lithiated with SLMP and tested to check if there was an improvement in the first cycle CE. Figure 4.4 (a) compares the first cycle potential profiles for the cells pressed at 100 psi with that of non-pre-lithiated, the results for which are recorded in Table 4.1. The CE improved to 55.79 % when 20 µl of SLMP was dropped on the electrodes. A further increase to 63.09 % was seen when SLMP was increased to 30 µl. The following observations can be made from the potential profiles in Figure 4.4:

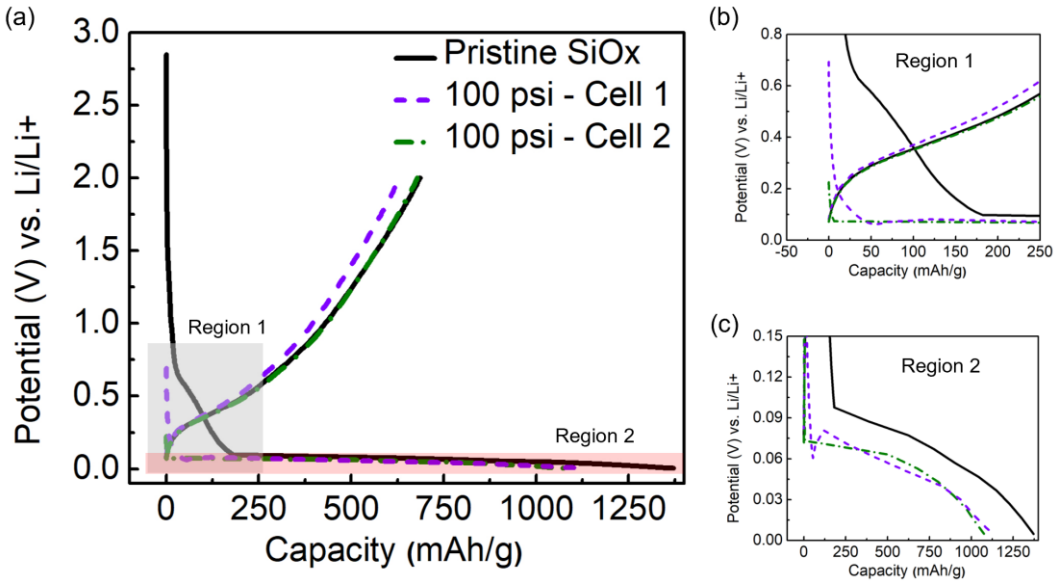

Figure 4.4. (a) Voltage profile for the 1st cycle for a SiO_x anode half cell in comparison with pre-lithiated SiO_x anodes at 100 psi. (b, c) Region 1 and 2 of the highlighted portions in (a).

Table 4.1. Comparison of electrochemical testing results for SiO_x anode half cells with and without SLMP pre-lithiation.

	Volume of SLMP solution (µl)	Pressure (psi)	1st Cycle Discharge Capacity (mAh/g)	1st Cycle Charge Capacity (mAh/g)	1st cycle CE (%)
Pristine SiO_x			1371.6831	685.6983	49.99
100 psi - Cell 1	20	100	1128.7833	629.7749	55.79
100 psi - Cell 2	30	100	1074.7081	678.1054	63.09
300 psi - Cell 1	20	300	1053.6926	705.9411	66.99
300 psi - Cell 2	30	300	1037.8872	691.2659	66.60

1. After assembly of cells, the OCV decreases with increasing amount of SLMP pre-lithiation (Figure 4.4(b)). The slope at the onset of discharge also decreases for 20 µl and vanishes for 30 µl trial. This indicates that SLMP has spontaneously reacted with SiO_x and formed the SEI eliminating the need for the irreversibility for the formation of SEI.
2. The capacity on discharge decreases with increase in deposition (Table 4.1). SLMP could be reacting with SiO_x to form silicates, oxides, or silicides, all of which are responsible for the discharge capacity in the first cycle.
3. Comparison of the lithiation plateau in Figure 4.4 (c) shows that the pre-lithiated cells discharge at a lower potential. This could be due to the increase in impedance at the interface due to SLMP.

The pressure activation step was increased from 100 psi to 300 psi to study the effect of pressure (Figure 4.5). The observations made for 100 psi apply also to 300 psi. However, the CE for 20 µl increased to 66.99 %. This indicates that a larger portion of SLMP is able to react with SiO_x when pressed at a higher pressure of 300 psi. Figure 4.5 (b) shows a lower OCV and no signs of the slope for 20 µl which is different from that seen in Figure 4.4 (b). When the amount of SLMP was increased to 30 µl, the CE was 66.60 %. It is possible that the utilization of SLMP is limited to the immediate surface of the electrode and increasing the amount does not mitigate the loss deep inside the electrode.

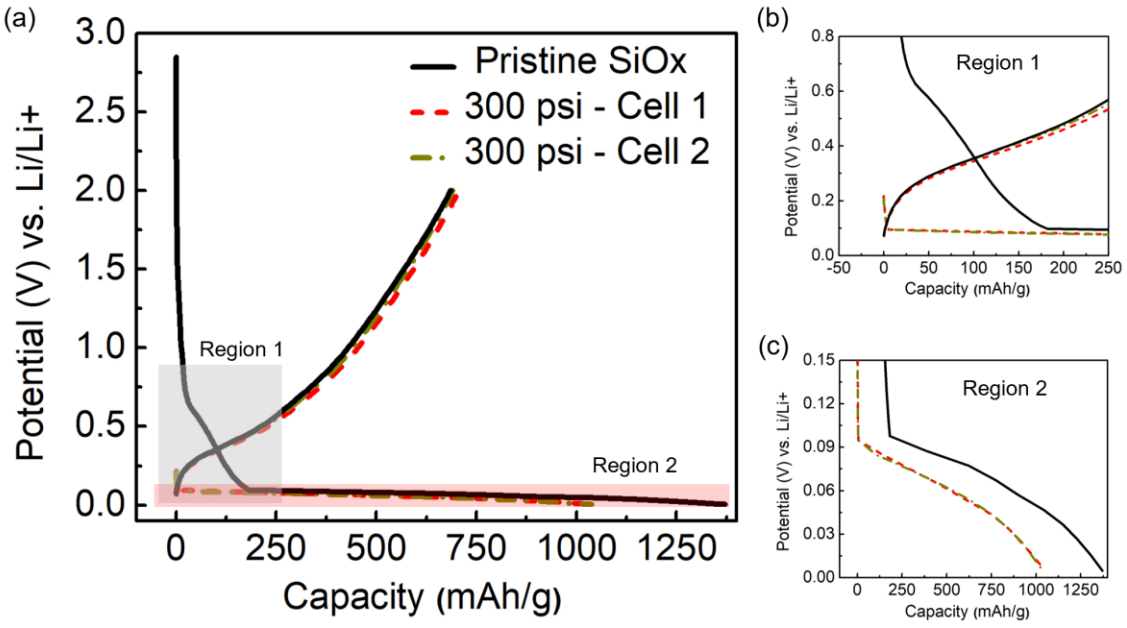

Figure 4.5. (a) Voltage profile for the 1st cycle for a SiO_x anode half cell in comparison with pre-lithiated SiO_x anodes at 300 psi. (b, c) Region 1 and 2 of the highlighted portions in (a).

4.4 Conclusion and Future Work

In this chapter, attempts were made to alleviate the first cycle capacity loss that is characteristic of SiO_x anode material. The SiO_x powder was first characterized to identify the morphology and elemental distribution of O, Si, and C in the sample. The material was also found to be amorphous. The electrochemical testing of SiO_x in half cells showed excellent stability with 94.81 % capacity retention over 100 cycles. However, the first cycle CE was only 49.99 %. SLMP was used to pre-lithiate the electrodes. Consequently, the CE increased to up to ~ 67 %. Furthermore, a higher pressure of 300 psi delivered a larger CE, hence, reducing the first cycle loss.

Pre-lithiation is an efficient technique to mitigate the first cycle loss. However, SLMP is an expensive product costing ~ 2000 $/kg. It is vital to find cost-effective methods to pre-lithiate SiO_x. Reports of alternatives on using Li salts such as LiOH, doping the material with metals such as Al, and surface coating techniques have shown promising results [63–66]. Work is in progress to identify a cost-effective alternative to SLMP.

Chapter 4 is coauthored with Yongbai Josh Gong, Dr. Pritesh Parikh, Dr. Abhik Banerjee, Osman Trieu, and Prof. Ying Shirley Meng. The thesis author is the primary author of this chapter.

Bibliography

1. Armand, M. & Tarascon, J. M. Building better batteries. *Nature* **451**, 652–657 (2008).

2. Tarascon, J. M. & Armand, M. Issues and challenges facing rechargeable lithium batteries. *Nature* **414**, 359–367 (2001).

3. Scrosati, B. & Garche, J. Lithium batteries: Status, prospects and future. *J. Power Sources* **195**, 2419–2430 (2010).

4. Roy, P. & Srivastava, S. K. Nanostructured anode materials for lithium ion batteries. *J. Mater. Chem. A* **3**, 2454–2484 (2015).

5. Winter, M., Barnett, B. & Xu, K. Before Li Ion Batteries. *Chem. Rev.* **118**, 11433–11456 (2018).

6. Wu, H. & Cui, Y. Designing nanostructured Si anodes for high energy lithium ion batteries. *Nano Today* **7**, 414–429 (2012).

7. Abraham, K. M. Prospects and limits of energy storage in batteries. *J. Phys. Chem. Lett.* **6**, 830–844 (2015).

8. Rahman, M. A., Song, G., Bhatt, A. I., Wong, Y. C. & Wen, C. Nanostructured silicon anodes for high-performance lithium-ion batteries. *Adv. Funct. Mater.* **26**, 647–678 (2016).

9. Ng, S. H., Wang, J., Wexler, D., Konstantinov, K., Guo, Z. P. & Liu, H. K. Highly reversible lithium storage in spheroidal carbon-coated silicon nanocomposites as anodes for lithium-ion batteries. *Angew. Chemie - Int. Ed.* **45**, 6896–6899 (2006).

10. Chan, C. K., Ruffo, R., Hong, S. S. & Cui, Y. Surface chemistry and morphology of the solid electrolyte interphase on silicon nanowire lithium-ion battery anodes. *J. Power Sources* **189**, 1132–1140 (2009).

11. Oumellal, Y., Delpuech, N., Mazouzi, D., Dupré, N., Gaubicher, J., Moreau, P., Soudan, P., Lestriez, B. & Guyomard, D. The failure mechanism of nano-sized Si-based negative electrodes for lithium ion batteries. *J. Mater. Chem.* **21**, 6201–6208 (2011).

12. Shobukawa, H., Alvarado, J., Yang, Y. & Meng, Y. S. Electrochemical performance and interfacial investigation on Si composite anode for lithium ion batteries in full cell. *J. Power Sources* **359**, 173–181 (2017).

13. Schroder, K., Alvarado, J., Yersak, T. A., Li, J., Dudney, N., Webb, L. J., Meng, Y. S. & Stevenson, K. J. The Effect of Fluoroethylene Carbonate as an Additive on the Solid Electrolyte Interphase on Silicon Lithium-Ion Electrodes. *Chem. Mater* 5531–5542 (2015).

14. Li, X., Gu, M., Hu, S., Kennard, R., Yan, P., Chen, X., Wang, C., Sailor, M. J., Zhang, J.-G. & Liu, J. Mesoporous silicon sponge as an anti-pulverization structure for high-performance lithium-ion battery anodes. *Nat. Commun.* **5**, 4105 (2014).

15. Chan, C. K., Peng, H., Liu, G., McIlwrath, K., Zhang, X. F., Huggins, R. A. & Cui, Y. High-performance lithium battery anodes using silicon nanowires. *Nat. Nanotechnol.* **3**, 31–35 (2008).

16. Liu, X. H., Zhong, L., Huang, S., Mao, S. X., Zhu, T. & Huang, J. Y. Size-dependent fracture of silicon nanoparticles during lithiation. *ACS Nano* **6**, 1522–1531 (2012).

17. Magasinski, A., Zdyrko, B., Kovalenko, I., Hertzberg, B., Burtovyy, R., Huebner, C. F., Fuller, T. F., Luzinov, I. & Yushin, G. Toward Efficient Binders for Li-Ion Battery Si-Based Anodes: Polyacrylic Acid. *ACS Appl. Mater. Interfaces* **2**, 3004–3010 (2010).

18. Choi, N., Ha, S., Lee, Y., Jang, J. Y., Jeong, M., Shin, W. C. & Ue, M. Recent Progress on Polymeric Binders for Silicon Anodes in Lithium-Ion Batteries. *J. Electrochem. Sci. Technol.* **6**, 35–49 (2015).

19. Chen, T., Wu, J., Zhang, Q. & Su, X. Recent advancement of SiOxbased anodes for lithium-ion batteries. *J. Power Sources* **363**, 126–144 (2017).

20. Dupré, N. D., Moreau, P., De Vito, E., Quazuguel, L., Boniface, M., Bordes, # A, Rudisch, ⊥ C, Bayle-Guillemaud, P. & Guyomard, D. Multiprobe Study of the Solid Electrolyte Interphase on Silicon-Based Electrodes in Full-Cell Configuration. *Chem. Mater.* **28**, 2557–2572 (2016).

21. Ye, J., Li, Y., Zhang, L., Zhang, X., Han, M., He, P. & Zhou, H. Fabrication and Performance of High Energy Li-Ion Battery Based on the Spherical Li[Li $_{0.2}$ Ni $_{0.16}$ Co $_{0.1}$ Mn $_{0.54}$]O $_{2}$ Cathode and Si Anode. *ACS Appl. Mater. Interfaces* **8**, 208–214 (2016).

22. Chae, C., Noh, H.-J., Lee, J. K., Scrosati, B. & Sun, Y.-K. A High-Energy Li-Ion Battery Using a Silicon-Based Anode and a Nano-Structured Layered Composite Cathode. *Adv. Funct. Mater.* **24**, 3036–3042 (2014).

23. Beattie, S. D., Loveridge, M. J., Lain, M. J., Ferrari, S., Polzin, B. J., Bhagat, R. & Dashwood, R. Understanding capacity fade in silicon based electrodes

for lithium-ion batteries using three electrode cells and upper cut-off voltage studies. *J. Power Sources* **302**, 426–430 (2016).

24. Shellikeri, A., Watson, V., Adams, D., Kalu, E. E., Read, J. A., Jow, T. R., Zheng, J. S. & Zheng, J. P. Investigation of Pre-lithiation in Graphite and Hard-Carbon Anodes Using Different Lithium Source Structures. *J. Electrochem. Soc.* **164**, 3914–3924 (2017).

25. Kasnatscheew, J., Placke, T., Streipert, B., Rothermel, S., Wagner, R., Meister, P., Laskovic, I. C. & Winter, M. A Tutorial into Practical Capacity and Mass Balancing of Lithium Ion Batteries. *J. Electrochem. Soc.* **164**, A2479–A2486 (2017).

26. Kwon, T.-W., Choi, J. W. & Coskun, A. The emerging era of supramolecular polymeric binders in silicon anodes. *Chem. Soc. Rev* **47**, 2145 (2018).

27. Sun, H. & Zhao, K. Electronic Structure and Comparative Properties of $LiNi_x Mn_y Co_z O_2$ Cathode Materials. *J. Phys. Chem. C* **121**, 6002–6010 (2017).

28. Amin, R. & Chiang, Y.-M. Characterization of Electronic and Ionic Transport in Li 1-x Ni 0.33 Mn 0.33 Co 0.33 O 2 (NMC 333) and Li 1-x Ni 0.50 Mn 0.20 Co 0.30 O 2 (NMC 523) as a Function of Li Content. *J. Electrochem. Soc.* **163**, 1512–1517 (2016).

29. Erk, C., Brezesinski, T., Sommer, H., Schneider, R. & Rgen Janek, J. Toward Silicon Anodes for Next-Generation Lithium Ion Batteries: A Comparative Performance Study of Various Polymer Binders and Silicon Nanopowders. *ACS Appl. Mater. Interfaces* **5**, 7299–7307 (2013).

30. Hu, B., Shkrob, I. A., Zhang, S., Zhang, L., Zhang, J., Li, Y., Liao, C., Zhang, Z., Lu, W. & Zhang, L. The existence of optimal molecular weight for poly(acrylic acid) binders in silicon/graphite composite anode for lithium-ion batteries. *J. Power Sources* **378**, 671–676 (2018).

31. Additive specialties and high performance concentrates Polymer Additives - AkzoNobel. (2016).

32. SuperP Li Carbon Black Additive - Timcal. (2019).

33. Nguyen, C. C., Seo, D. M., Chandrasiri, K. W. D. K. & Lucht, B. L. Improved Cycling Performance of a Si Nanoparticle Anode Utilizing Citric Acid as a Surface-Modifying Agent. *ACS Langmuir* **33**, 9254–9261 (2016).

34. Parikh, P., Sina, M., Banerjee, A., Wang, X., Savio, M., Souza, D. ', Doux, J.-M., Wu, E. A., Trieu, O. Y., Gong, Y., Zhou, Q., Snyder, K. & Meng, Y. S. Role of Polyacrylic Acid (PAA) Binder on the Solid Electrolyte Interphase in Silicon

Anodes. *Chem. Mater.* **31**, 2535–2544 (2019).

35. Ender, M., Weber, A. & Ivers-Tiffée, E. Analysis of Three-Electrode Setups for AC-Impedance Measurements on Lithium-Ion Cells by FEM simulations. *J. Electrochem. Soc.* **159**, A128 (2012).

36. Hoshi, Y., Narita, Y., Honda, K., Ohtaki, T., Shitanda, I. & Itagaki, M. Optimization of reference electrode position in a three-electrode cell for impedance measurements in lithium-ion rechargeable battery by finite element method. *J. Power Sources* **288**, 168–175 (2015).

37. Jung, R., Metzger, M., Maglia, F., Stinner, C. & Gasteiger, H. A. Oxygen Release and Its Effect on the Cycling Stability of LiNi x Mn y Co z O 2 (NMC) Cathode Materials for Li-Ion Batteries. *J. Electrochem. Soc.* **164**, 1361–1377 (2017).

38. Jung, R., Metzger, M., Maglia, F., Stinner, C. & Gasteiger, H. A. Chemical versus Electrochemical Electrolyte Oxidation on NMC111, NMC622, NMC811, LNMO, and Conductive Carbon. *J. Phys. Chem. Lett* **8**, 4820–4825 (2017).

39. Jung, S.-K., Gwon, H., Hong, J., Park, K.-Y., Seo, D.-H., Kim, H., Hyun, J., Yang, W. & Kang, K. Understanding the Degradation Mechanisms of $LiNi_{0.5}Co_{0.2}Mn_{0.3}O_2$ Cathode Material in Lithium Ion Batteries. *Adv. Energy Mater.* **4**, 1300787 (2014).

40. Wu, L., Nam, K.-W., Wang, X., Zhou, Y., Zheng, J.-C., Yang, X.-Q. & Zhu, Y. Structural Origin of Overcharge-Induced Thermal Instability of Ni-Containing Layered-Cathodes for High-Energy-Density Lithium Batteries. *Chem. Mater* **23**, 3953–3960 (2011).

41. Mohanty, D. & Gabrisch, H. Microstructural investigation of LixNi1/3Mn1/3Co1/3O2 (x ≤ 1) and its aged products via magnetic and diffraction study. *J. Power Sources* **220**, 405–412 (2012).

42. Mohanty, D., Kalnaus, S., Meisner, R. A., Rhodes, K. J., Li, J., Payzant, E. A., Wood, D. L. & Daniel, C. Structural transformation of a lithium-rich Li 1.2 Co 0.1 Mn 0.55 Ni 0.15 O 2 cathode during high voltage cycling resolved by in situ X-ray diffraction. *J. Power Sources* **229**, 239–248 (2013).

43. Kwon, T., Kyeong Jeong, Y., Lee, I., Kim, T.-S., Wook Choi, J., Coskun, A., Kwon, T., Jeong, Y. K., Choi, J. W., Lee, I., Kim, T. & Coskun, A. Systematic Molecular-Level Design of Binders Incorporating Meldrum's Acid for Silicon Anodes in Lithium Rechargeable Batteries. *Adv. Mater.* **26**, 7979–7985 (2014).

44. Zhang, L., Bailey, J. B., Subramanian, R. H. & Tezcan, F. A. Hyperexpandable, self-healing macromolecular crystals with integrated polymer networks. *Nature* **557**, 86–91 (2018).

45. Taddese, T., Carbone, P. & Cheung, D. L. Thermodynamics of linear and star polymers at fluid interfaces. *Soft Matter* **11**, 81–93 (2015).

46. Lee, B.-R., Ko, H. K., Ryu, J. H., Ahn, K. Y., Lee, Y.-H., Oh, J., Na, J. H., Kim, T. W., Byun, Y., Kwon, I. C., Kim, K. & Lee, J. Engineered Human Ferritin Nanoparticles for Direct Delivery of Tumor Antigens to Lymph Node and Cancer Immunotherapy. *Sci. Rep.* **6**, 35182 (2016).

47. Kim, S.-W., Kim, Y.-H. & Lee, J. Thermal Stability of Human Ferritin: Concentration Dependence and Enhanced Stability of an N-Terminal Fusion Mutant. *Biochem. Biophys. Res. Commun.* **289**, 125–129 (2001).

48. Yuan, T. Z., Ormonde, C. F. G., Kudlacek, S. T., Kunche, S., Smith, J. N., Brown, W. A., Pugliese, K. M., Olsen, T. J., Iftikhar, M., Raston, C. L. & Weiss, G. A. Shear-stress-mediated refolding of proteins from aggregates and inclusion bodies. *ChemBioChem* **16**, 393–396 (2015).

49. Liu, Z., Yu, Q., Zhao, Y., He, R., Xu, M., Feng, S., Li, S., Zhou, L. & Mai, L. Silicon oxides: a promising family of anode materials for lithium-ion batteries. *Chem. Soc. Rev* **48**, 285 (2019).

50. Aravindan, V., Lee, Y. S. & Madhavi, S. Best Practices for Mitigating Irreversible Capacity Loss of Negative Electrodes in Li-Ion Batteries. *Adv. Energy Mater.* **7**, 1602607 (1-17) (2017).

51. Kitada, K., Pecher, O., Magusin, P. C. M. M., Groh, M. F., Weatherup, R. S. & Grey, C. P. Unraveling the Reaction Mechanisms of SiO Anodes for Li-Ion Batteries by Combining in Situ 7 Li and ex Situ 7 Li/ 29 Si Solid-State NMR Spectroscopy. *J. Am. Chem. Soc.* **141**, 7014–7027 (2019).

52. Varzi, A., Bresser, D., von Zamory, J., Müller, F., Passerini, S., Varzi, A., Bresser, D., von Zamory, J., Müller, F. & Passerini, S. ZnFe2O4-C/LiFePO4-CNT: A Novel High-Power Lithium-Ion Battery with Excellent Cycling Performance. *Adv. Energy Mater.* **4**, 1400054 (1 to 9) (2014).

53. Scott, M. G., Whitehead, A. H. & Owen, J. R. Chemical Formation of a Solid Electrolyte Interface on the Carbon Electrode of a Li-Ion Cell. *J. Electrochem. Soc.* **145**, 1506–1510 (1998).

54. Marinaro, M., Weinberger, M. & Wohlfahrt-Mehrens, M. Toward pre-lithiatied high areal capacity silicon anodes for Lithium-ion batteries. *Electrochim. Acta* **206**, 99–107 (2016).

55. Liu, N., Hu, L., McDowell, M. T., Jackson, A. & Cui, Y. Prelithiated silicon nanowires as an anode for lithium ion batteries. *ACS Nano* **5**, 6487–6493 (2011).

56. Forney, M. W., Ganter, M. J., Staub, J. W., Ridgley, R. D. & Landi, B. J. Prelithiation of silicon-carbon nanotube anodes for lithium ion batteries by stabilized lithium metal powder (SLMP). *Nano Lett.* **13**, 4158–4163 (2013).

57. Wang, Z., Fu, Y., Zhang, Z., Yuan, S., Amine, K., Battaglia, V. & Liu, G. Application of Stabilized Lithium Metal Powder (SLMP®) in graphite anode - A high efficient prelithiation method for lithium-ion batteries. *J. Power Sources* **260**, 57–61 (2014).

58. Xiang, B., Wang, L., Liu, G. & Minor, A. M. Electromechanical Probing of Li/Li 2 CO 3 Core/Shell Particles in a TEM. *J. Electrochem. Soc.* **160**, 415–419 (2013).

59. Yang, X., Wen, Z., Xu, X., Lin, B. & Huang, S. Nanosized silicon-based composite derived by in situ mechanochemical reduction for lithium ion batteries. *J. Power Sources* **164**, 880–884 (2007).

60. Seong, I. W., Kim, K. T. & Yoon, W. Y. Electrochemical behavior of a lithium-pre-doped carbon-coated silicon monoxide anode cell. *J. Power Sources* **189**, 511–514 (2009).

61. Seong, I. W. & Yoon, W. Y. Electrochemical behavior of a silicon monoxide and Li-powder double layer anode cell. *J. Power Sources* **195**, 6143–6147 (2010).

62. Zhao, H., Wang, Z., Lu, P., Jiang, M., Shi, F., Song, X., Zheng, Z., Zhou, X., Fu, Y., Abdelbast, G., Xiao, X., Liu, Z., Battaglia, V. S., Zaghib, K. & Liu, G. Toward Practical Application of Functional Conductive Polymer Binder for a High-Energy Lithium-Ion Battery Design. *Nano Lett.* **14**, 6704–6710 (2014).

63. Veluchamy, A., Doh, C.-H., Kim, D.-H., Lee, J.-H., Lee, D.-J., Ha, K.-H., Shin, H.-M., Jin, B.-S., Kim, H.-S., Moon, S.-I. & Park, C.-W. Improvement of cycle behaviour of SiO/C anode composite by thermochemically generated Li 4 SiO 4 inert phase for lithium batteries. *J. Power Sources* **188**, 574–577 (2009).

64. Zhang, Y., Guo, G., Chen, C., Jiao, Y., Li, T., Chen, X., Yang, Y., Yang, D. & Dong, A. An affordable manufacturing method to boost the initial Coulombic efficiency of disproportionated SiO lithium-ion battery anodes. *J. Power Sources* **426**, 116–123 (2019).

65. Cui, J., Yang, J., Man, J., Li, S., Yin, J., Ma, L., He, W., Sun, J. & Hu, J. Porous Al/Al2O3 two-phase nanonetwork to improve electrochemical properties of

porous C/SiO2 as anode for Li-ion batteries. *Electrochim. Acta* **300**, 470–481 (2019).

66. Miyachi, M., Yamamoto, H. & Kawai, H. Electrochemical Properties and Chemical Structures of Metal-Doped SiO Anodes for Li-Ion Rechargeable Batteries. *J. Electrochem. Soc.* **154**, A376–A380 (2007).